

The syntheses, structures and spectroelectrochemical properties of 6-oxo-verdazyl derivatives bearing surface anchoring groups

Varshini J. Kumar,^a† Jian-Zhong Wu,^{b*}† Martyna Judd,^c Elodie Rousset,^a Marcus Korb,^a Stephen A. Moggach,^a Nicholas Cox,^c Paul J. Low^{a*}

^a School of Molecular Sciences, University of Western Australia, 35 Stirling Highway, Crawley, Western Australia, 6009, Australia, paul.low@uwa.edu.au

^b School of Chemistry, South China Normal University, Guangzhou 510006, China, wujzh@scnu.edu.cn

^c Research School of Chemistry, Australian National University, Canberra, ACT, 2601, Australia

† These authors contributed equally

CONTENTS

Figure S1. A plot of the crystallographically determined molecular structure of **2a** with thermal ellipsoids drawn at 50% probability. Hydrogen atoms omitted for clarity. Selected bond lengths (Å) and angles (°): C1-Cl1, 1.777(2); C1-O1, 1.197(2); C1-N1, 1.356(2); N1-C9, 1.449(2); N1-N2, 1.390(2); N2-C2, 1.276(2); C2-C3, 1.470(2); Cl1-C1-O1, 120.0(2); O1-C1-N1, 126.1(2); C1-N1-C9, 118.8(2); C1-N1-N2, 118.8(2); N1-N2-C2, 118.8(2); N2-C2-C3, 118.6(1). 4

Figure S2. A plot of the crystallographically determined molecular structure of **3a** with thermal ellipsoids drawn at 50% probability. Selected hydrogen atoms omitted for clarity. 4

Figure S3. a) Plots of the crystallographically determined molecular structure of **3c** with thermal ellipsoids at 20%, for molecule 1 (top) and molecule 2 (bottom) of the asymmetric unit. b) Spatial arrangement of the two molecules in the asymmetric unit, forming an angle of 70(1)° between the two mean plane containing the four nitrogen atoms. Selected hydrogen atoms omitted for clarity. 5

Figure S4. A plot of the crystallographically determined molecular structure of **4a** with thermal ellipsoids drawn at 50% probability. Hydrogen atoms omitted for clarity. 6

Figure S5. A plot of the crystallographically determined molecular structure of **4c** with thermal ellipsoids drawn at 50% probability. Hydrogen atoms omitted for clarity. 6

Table S1. Crystal structure and refinement details 7

Table S2. Summary of TD-DFT results from the model compound 2,4,6-triphenyl-1,2,4,5-tetrazinan-3-one (**A**) (B3LYP / 6-31G*(df,p) / COSMO(CPCM) (CH₂Cl₂). 8

Table S3. Summary of TD-DFT results from the model compound 1,3,5-triphenyl-6-oxo-verdazyl (**B**) (B3LYP / 6-31G*(df,p) / COSMO(CPCM) (CH₂Cl₂). 9

Table S4. Summary of TD-DFT results from the model compound 1,5-bis(phenylethynyl)-3-phenyl-6-oxo-verdazyl (**C**) (B3LYP / 6-31G*(df,p) / COSMO(CPCM) (CH₂Cl₂). 11

Figure S6. The UV-vis spectra ($\tilde{\nu}_{max}$ / cm⁻¹ (ϵ / M⁻¹cm⁻¹)) of tetrazines **3a - c, 5, 6** and **7..13**

Figure S7. The UV-vis spectra ($\tilde{\nu}_{max}$ / cm ⁻¹ (ϵ / M ⁻¹ cm ⁻¹) of verdazyls 4a - c , 8 , 9 and 10..14	14
Figure S8. Plots of the spin density from the model verdazyl radical (a) [B] (b) [C]	15
Figure S9. Cyclic Voltammograms of compounds 4a - c and 8 - 10 in 0.1 M NBu ₄ PF ₆ / CH ₂ Cl ₂ solution. Voltammograms are plotted vs ferrocene/ferrocenium ($E_{1/2} = 0$ V) from data collected against an decamethylferrocene / decamethylferrocenium internal reference couple ($E_{1/2} = -0.55$ V)	16
Figure S10. Square Wave Voltammograms of compounds 4a - c and 8 - 10 in 0.1 M NBu ₄ PF ₆ / CH ₂ Cl ₂ solution. Voltammograms are plotted vs ferrocene/ferrocenium ($E_{1/2} = 0$ V) from data collected against a decamethylferrocene / decamethylferrocenium internal reference couple ($E_{1/2} = -0.55$ V)	17
Table S5. Summary of UV-vis-NIR spectroelectrochemical data for compounds 4a-c , 9 and 10	18
Figure S11. Plots of spectroelectrochemical data of 4b in the UV-vis-NIR region	19
Figure S12. Plots of spectroelectrochemical data of 4c in the UV-vis-NIR region	19
Figure S13. The spectroelectrochemically generated spectra of [10]⁻	19
Figure S14. The ¹ H NMR spectrum of 3a	20
Figure S15. The ¹³ C{ ¹ H} NMR spectrum of 3a	21
Figure S16. The mass spectrum of 3a	22
Figure S17. The mass spectrum of 4a	23
Figure S18. The ¹ H NMR spectrum of 3b . The inset shows an expansion of the aromatic region for clarity	24
Figure S19. The ¹³ C{ ¹ H} NMR spectrum of 3b .	25
Figure S20. The mass spectrum of 3b	26
Figure S21. The mass spectrum of 4b	27
Figure S22. The ¹ H NMR spectrum of 3c . The inset shows an expansion of the aromatic region for clarity	28
Figure S23. The ¹³ C{ ¹ H} NMR spectrum of 3c .	29
Figure S24. The mass spectrum of 3c	30
Figure S25. The mass spectrum of 4c	31
Figure S26. The ¹ H NMR spectrum of 5 . The inset shows an expansion of the aromatic region for clarity	32
Figure S27. The ¹³ C{ ¹ H} NMR spectrum of 5	33
Figure S28. The mass spectrum of 5	34
Figure S29. The ¹ H NMR spectrum of 6 . The inset shows an expansion of the aromatic region for clarity	35
Figure S30. The ¹³ C{ ¹ H} NMR spectrum of 6	36
Figure S31. The mass spectrum of 6	37
Figure S32. The ¹ H NMR spectrum of 7 . The inset shows an expansion of the aromatic region for clarity	38

Figure S33. The $^{13}\text{C}\{^1\text{H}\}$ NMR spectrum of 7	39
Figure S34. The mass spectrum of 7	40
Figure S35. The mass spectrum of 8	41
Figure S36. The mass spectrum of 9	42
Figure S37. The mass spectrum of 10	43
Additional EPR materials and Methods	44

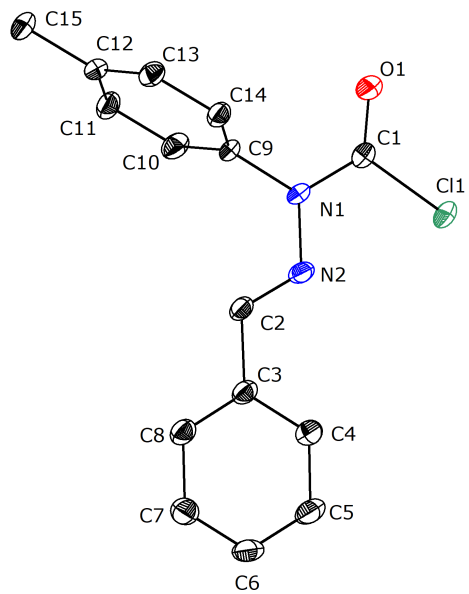


Figure S1. A plot of the crystallographically determined molecular structure of **2a** with thermal ellipsoids drawn at 50% probability. Hydrogen atoms omitted for clarity. Selected bond lengths (\AA) and angles ($^{\circ}$): C1-C11, 1.777(2); C1-O1, 1.197(2); C1-N1, 1.356(2); N1-C9, 1.449(2); N1-N2, 1.390(2); N2-C2, 1.276(2); C2-C3, 1.470(2); C11-C1-O1, 120.0(2); O1-C1-N1, 126.1(2); C1-N1-C9, 118.8(2); C1-N1-N2, 118.8(2); N1-N2-C2, 118.8(2); N2-C2-C3, 118.6(1).

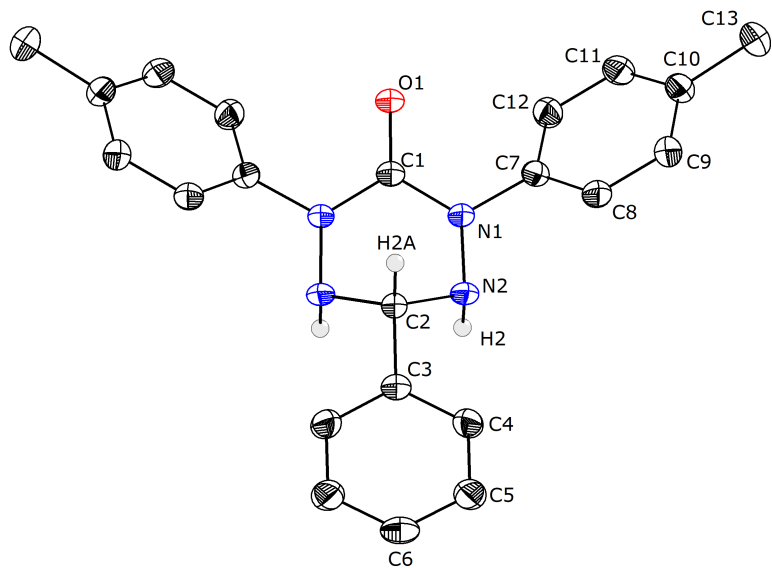


Figure S2. A plot of the crystallographically determined molecular structure of **3a** with thermal ellipsoids drawn at 50% probability. Selected hydrogen atoms omitted for clarity.

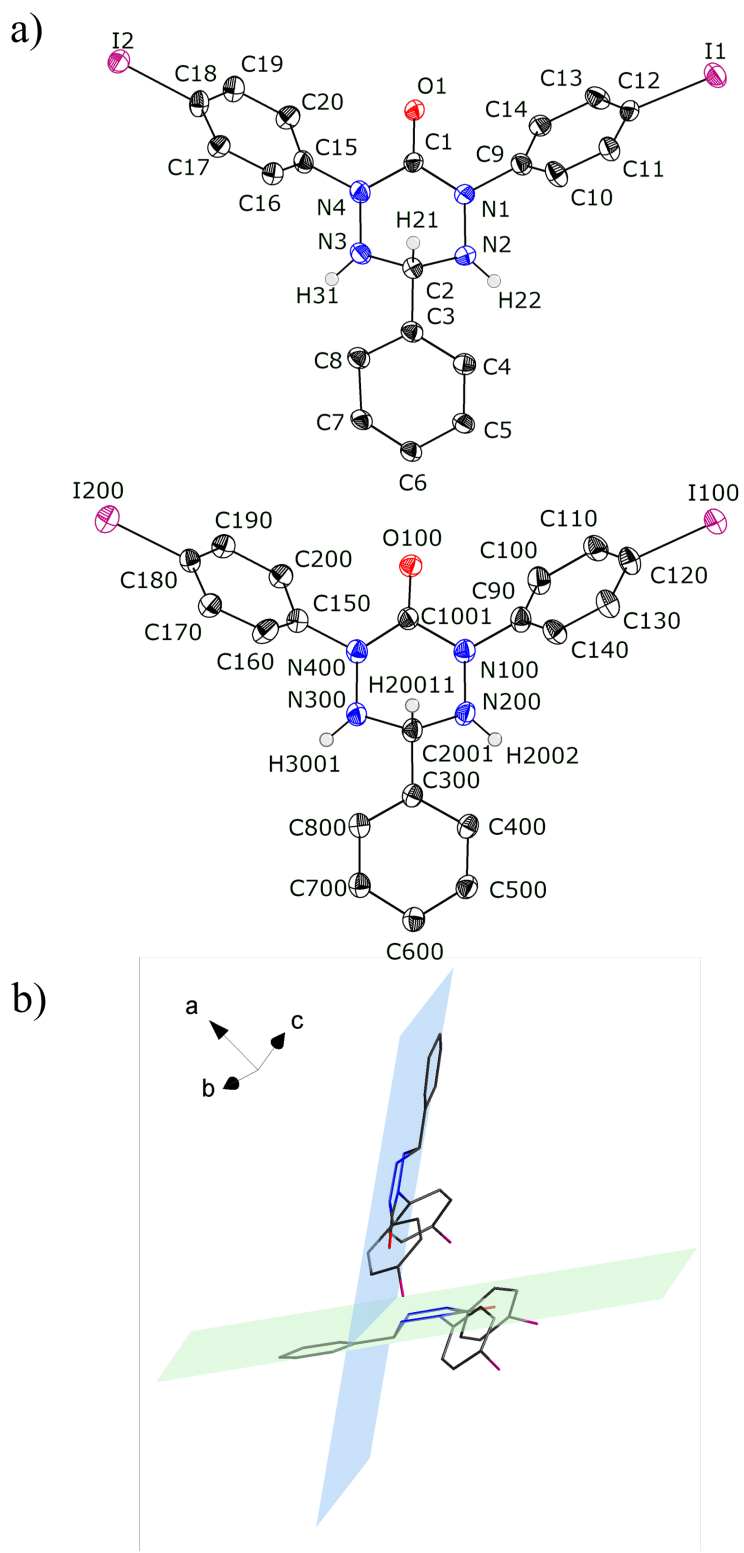


Figure S3. a) Plots of the crystallographically determined molecular structure of **3c** with thermal ellipsoids at 20%, for molecule 1 (top) and molecule 2 (bottom) of the asymmetric unit. b) Spatial arrangement of the two molecules in the asymmetric unit, forming an angle of $70(1)^\circ$ between the two mean plane containing the four nitrogen atoms. Selected hydrogen atoms omitted for clarity.

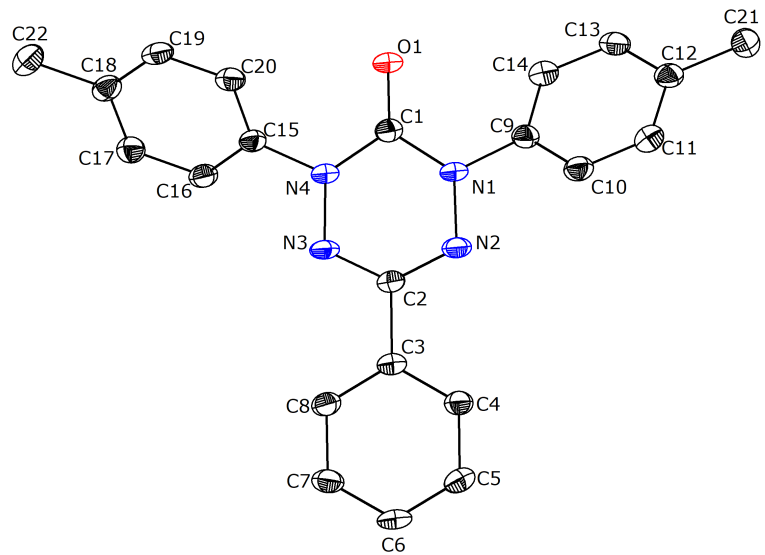


Figure S4. A plot of the crystallographically determined molecular structure of **4a** with thermal ellipsoids drawn at 50% probability. Hydrogen atoms omitted for clarity.

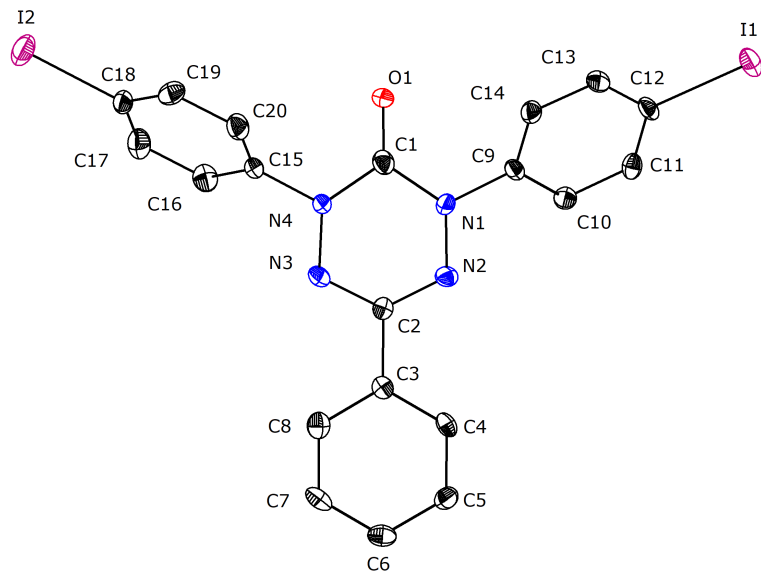


Figure S5. A plot of the crystallographically determined molecular structure of **4c** with thermal ellipsoids drawn at 50% probability. Hydrogen atoms omitted for clarity.

Table S1. Crystal structure and refinement details

	2a	3a	3b	3c	4a	4b	4c
CCDC Number	2109616	2109617	2109618	2109619	2109620	2109621	2109622
Empirical formula	C ₁₅ H ₁₃ ClN ₂ O	C ₂₂ H ₂₂ N ₄ O	C ₂₄ H ₂₄ Cl ₆ N ₄ OS ₂	C ₂₀ H ₁₆ I ₂ N ₄ O	C ₂₂ H ₁₉ N ₄ O	C ₂₂ H ₁₉ N ₄ OS ₂	C ₂₀ H ₁₃ I ₂ N ₄ O
Formula weight	272.72	358.43	661.29	582.18	355.41	419.53	579.14
Temperature/K	99.8(7)	99.8(6)	99.9(6)	100	99.8(6)	99.9(4)	99.95(10)
Crystal system	<i>monoclinic</i>	<i>monoclinic</i>	<i>monoclinic</i>	<i>triclinic</i>	<i>monoclinic</i>	<i>monoclinic</i>	<i>triclinic</i>
Space group	P2 ₁ /c	P2 ₁ /m	I2/a	P-1	P2 ₁ /n	P2 ₁ /c	P-1
<i>a</i> /Å	8.9460(2)	5.1113(2)	24.2469(4)	8.6930(5)	7.1902(2)	7.2557(2)	4.0177(2)
<i>b</i> /Å	11.1772(3)	22.2891(9)	5.37710(10)	12.8412(7)	11.2885(3)	24.1715(7)	10.1392(5)
<i>c</i> /Å	13.8578(3)	8.3663(4)	44.3688(11)	18.8190(8)	21.8846(7)	11.2028(3)	23.1774(9)
<i>α</i> /°	90	90	90	74.349(4)	90	90	87.900(4)
<i>β</i> /°	100.517(2)	105.156(5)	95.275(2)	82.296(4)	90.343(3)	93.330(2)	86.840(4)
<i>γ</i> /°	90	90	90	79.321(5)	90	90	80.762(4)
<i>V</i> /Å ³	1362.38(6)	919.99(7)	5760.2(2)	1979.95(18)	1776.27(9)	1961.44(9)	930.13(8)
<i>Z</i>	4	2	8	4	4	4	2
<i>Q</i> _{calc} g/cm ³	1.33	1.294	1.525	1.953	1.329	1.421	2.068
μ/mm ⁻¹	2.421	0.65	7.02	25.092	0.672	2.636	3.399
<i>F</i> (000)	568	380	2704	1112	748	876	550.0
Crystal size/mm ³	0.051×0.034×0.028	0.196×0.066×0.042	0.286×0.064×0.056	0.181×0.044×0.039	0.244×0.111×0.057	0.434×0.155×0.138	0.20×0.10×0.01
Radiation	CuKα (λ = 1.54184)	CuKα (λ = 1.54184)	CuKα (λ = 1.54184)	Cu Kα (λ = 1.54184)	CuKα (λ = 1.54184)	CuKα (λ = 1.54184)	MoKα (λ = 0.71073)
2Θ range for data collection/°	10.056 to 149.984	7.934 to 150.656	7.322 to 151.39	4.896 to 90.048	8.08 to 150.192	7.314 to 152.622	6.58 to 52
Index ranges	-9 ≤ <i>h</i> ≤ 11, -13 ≤ <i>k</i> ≤ 13, -17 ≤ <i>l</i> ≤ 17	-6 ≤ <i>h</i> ≤ 5, -27 ≤ <i>k</i> ≤ 27, -10 ≤ <i>l</i> ≤ 10	-30 ≤ <i>h</i> ≤ 30, -5 ≤ <i>k</i> ≤ 6, -54 ≤ <i>l</i> ≤ 54	-7 ≤ <i>h</i> ≤ 7, -11 ≤ <i>k</i> ≤ 11, -17 ≤ <i>l</i> ≤ 17	-8 ≤ <i>h</i> ≤ 6, -13 ≤ <i>k</i> ≤ 13, -26 ≤ <i>l</i> ≤ 27	-9 ≤ <i>h</i> ≤ 7, -29 ≤ <i>k</i> ≤ 30, -14 ≤ <i>l</i> ≤ 14	-4 ≤ <i>h</i> ≤ 4, -12 ≤ <i>k</i> ≤ 12, -28 ≤ <i>l</i> ≤ 28
Reflections collected	24984	13294	99682	31524	15068	36258	6834
Independent reflections	2755 [<i>R</i> _{int} = 0.0777, <i>R</i> _o = 0.0355]	1927 [<i>R</i> _{int} = 0.0806, <i>R</i> _o = 0.0416]	5808 [<i>R</i> _{int} = 0.1425, <i>R</i> _o = 0.0371]	3153 [<i>R</i> _{int} = 0.158, <i>R</i> _{sigma} = 0.089]	3465 [<i>R</i> _{int} = 0.0855, <i>R</i> _o = 0.0611]	3996 [<i>R</i> _{int} = 0.1463, <i>R</i> _o = 0.0564]	6834 [<i>R</i> _{int} = 0.0514, <i>R</i> _o = 0.0593]
Data/restraints/parameters	2755/0/173	1927/0/137	5808/0/336	3153/504/489	3465/0/246	3996/0/264	6834/0/245
Goodness-of-fit on <i>F</i> ²	1.063	1.112	1.089	0.992	1.034	1.074	0.877
Final <i>R</i> indexes [<i>I</i> ≥ 2σ(<i>I</i>)]	<i>R</i> ₁ = 0.0394, <i>wR</i> ₂ = 0.0938	<i>R</i> ₁ = 0.0509, <i>wR</i> ₂ = 0.1427	<i>R</i> ₁ = 0.0755, <i>wR</i> ₂ = 0.2033	<i>R</i> ₁ = 0.1055, <i>wR</i> ₂ = 0.2719	<i>R</i> ₁ = 0.0568, <i>wR</i> ₂ = 0.1476	<i>R</i> ₁ = 0.0589, <i>wR</i> ₂ = 0.1612	<i>R</i> ₁ = 0.0355, <i>wR</i> ₂ = 0.0781
Final <i>R</i> indexes [all data]	<i>R</i> ₁ = 0.0445, <i>wR</i> ₂ = 0.0967	<i>R</i> ₁ = 0.0600, <i>wR</i> ₂ = 0.1585	<i>R</i> ₁ = 0.0801, <i>wR</i> ₂ = 0.2077	<i>R</i> ₁ = 0.1187, <i>wR</i> ₂ = 0.2812	<i>R</i> ₁ = 0.0673, <i>wR</i> ₂ = 0.1590	<i>R</i> ₁ = 0.0657, <i>wR</i> ₂ = 0.1758	<i>R</i> ₁ = 0.0598, <i>wR</i> ₂ = 0.0821
Largest diff. peak/hole / e Å ⁻³	0.30/-0.27	0.26/-0.26	0.53/-0.66	1.91/-1.31	0.30/-0.40	0.47/-0.70	1.19/-0.81

Table S2. Summary of TD-DFT results from the model compound 2,4,6-triphenyl-1,2,4,5-tetrazinan-3-one (**A**) (B3LYP / 6-31G*(df,p) / COSMO(CPCM) (CH₂Cl₂).

λ_1 / cm ⁻¹	<i>f</i>	assignment	X	Y	Z	N1	N2H	C _{Ph} H	N3H	N4	CO
A											
34691	0.3636	HOMO – LUMO	21 → 24 (3)	21 → 24 (3)	0 → 28 (28)	14 → 4 (-10)	14 → -3 (-17)	1 → 9 (8)	14 → -2 (-16)	14 → 4 (-10)	2 → 12 (10)

Table S3. Summary of TD-DFT results from the model compound 1,3,5-triphenyl-6-oxo-verdazyl (**B**) (B3LYP / 6-31G*(df,p) / COSMO(CPCM) (CH₂Cl₂).

λ / cm^{-1}	f	assignment	X	Y	Z	N1	N2	C _{Ph}	N3	N4	CO
B											
18937	0.0495	$\beta\text{-HOMO}-$	9→6	9→6	36→7	7→12	6→26	7→3	6→26	7→12	12→3
		$\beta\text{-LUMO}$	(-3)	(-3)	(-29)	(5)	(20)	(-4)	(20)	(5)	(-9)
21606	0.0076	[$\beta\text{-HOMO-1}$]−	23→6	23→6	7→2	2→14	12→29	3→1	12→29	2→14	14→0
		[$\beta\text{-LUMO}$]	(-17)	(-17)	(-5)	(12)	(17)	(-2)	(17)	(12)	(-14)
23099	0.0166	$\alpha\text{-HOMO}-$	12→4	1→24	6→38	15→3	19→9	1→16	19→9	15→3	2→15
		$\alpha\text{-LUMO}$	(-8)	(-8)	(32)	(-12)	(-10)	(15)	(-10)	(-12)	(13)
29148	0.1831	$\alpha\text{-HOMO}-$	19→31	19→31	10→9	10→4	14→5	1→2	14→5	10→4	2→7
		[$\alpha\text{-LUMO+1}$]	(12)	(12)	(-1)	(-6)	(-9)	(1)	(-9)	(-6)	(5)
36751	0.2493	[$\alpha\text{-HOMO-1}$]−	12→11	12→11	51→44	4→1	3→5	3→10	3→5	4→1	9→12
		[$\alpha\text{-LUMO}$]	(-1)	(-1)	(-7)	(-3)	(2)	(7)	(2)	(-3)	(3)
37219	0.2406	[$\alpha\text{-HOMO-1}$]−									
		[$\alpha\text{-LUMO}$]									
		$\beta\text{-HOMO}-$	17→20	17→20	36→35	5→1	5→3	3→8	5→3	5→1	7→10
		[$\beta\text{-LUMO+1}$]	(3)	(3)	(-1)	(-4)	(-2)	(5)	(-2)	(-4)	(3)
[B]⁺											
14259	0.1036	HOMO −	11→9	11→9	53→1	3→16	4→24	2→1	4→24	3→16	9→0
		LUMO	(-2)	(-2)	(-52)	(13)	(20)	(-1)	(20)	(13)	(-9)
19004	0.3711	[HOMO-3]−									
		LUMO									
		[HOMO-4]−	40→9	16→1	0→16	1→24	0→1	1→24	0→16	0→0	40→9
		LUMO	(-31)	(-15)	(16)	(23)	(1)	(23)	(16)	(0)	(-31)
19580	0.0325	[HOMO-5]−									
		LUMO									
		[HOMO-6]−	25→9	25→9	2→1	2→16	13→24	3→1	13→24	2→16	15→0
		LUMO	(-16)	(-16)	(-1)	(14)	(11)	(-2)	(11)	(14)	(-15)
22850	0.1002	[HOMO-5]−	22→9	22→9	2→1	3→16	14→24	3→1	14→24	3→16	17→0

		LUMO [HOMO-6] - LUMO	(-13)	(-13)	(-1)	(13)	(10)	(-2)	(10)	(13)	(-17)
33665	0.5114	HOMO - [LUMO+1]	11→2 (-9)	11→2 (-9)	54→27 (- 27)	3→1 (-2)	4→7 (3)	2→21 (19)	4→7 (3)	3→1 (-2)	9→33 (24)
[B]⁻											
19428	0.0131	HOMO - LUMO	9→5 (-4)	9→5 (-4)	1→58 (57)	12→0 (-12)	28→6 (-22)	1→8 (7)	28→6 (-22)	12→0 (-12)	0→13 (13)
22644	0.4037	HOMO - [LUMO+1]	9→36 (27)	9→36 (27)	1→10 (9) (-11)	12→1 (-27)	28→1 (1)	1→2 (-27)	28→1 (-27)	12→1 (-11)	0→13 (13)
24896	0.0794	HOMO - [LUMO+2]	9→2 (-7)	9→2 (-7)	1→95 (94)	12→0 (-12)	28→1 (-27)	1→0 (-1)	28→1 (-27)	12→0 (-12)	0→0 (0)
29048	0.0715	HOMO - [LUMO+5]	9→45 (36)	9→45 (36)	1→3 (2)	12→3 (-9)	28→1 (-27)	1→1 (0)	28→1 (-27)	12→3 (-9)	0→-3 (-3)
36685	0.2834	[HOMO-1] - LUMO	16→10 (-6)	16→10 (-6)	19→54 (35)	8→0 (-8)	6→5 (-1)	6→7 (1)	6→5 (-1)	8→0 (-8)	15→8 (-7)

Table S4. Summary of TD-DFT results from the model compound 1,5-bis(phenylethynyl)-3-phenyl-6-oxo-verdazyl (**C**) (B3LYP / 6-31G*(df,p) / COSMO(CPCM) (CH₂Cl₂).

λ / cm^{-1}	f	assignment	X	Y	Z	N1	N2	C _{Ph}	N3	N4	CO
C											
17104	0.2234	$\beta\text{-HOMO}-$	37→11	37→11	10→2	2→11	2→25	2→2	2→25	2→11	5→1
		$\beta\text{-LUMO}$	(-26)	(-26)	(-8)	(9)	(23)	(0)	(23)	(9)	(-4)
18630	0.0464	[$\beta\text{-HOMO-1}$] –	44→16	44→16	1→1	1→10	3→23	0→1	3→23	1→10	2→1
		[$\beta\text{-LUMO}$]	(-28)	(-28)	(0)	(9)	(20)	(1)	(20)	(9)	(-1)
22208	0.3422	$\alpha\text{-HOMO}-$									
		$\alpha\text{-LUMO}$	27→27	27→27	15→5	6→5	7→12	2→2	7→12	6→5	3→4
		[$\beta\text{-HOMO-2}$] –	(0)	(0)	(-10)	(-1)	(5)	(0)	(5)	(-1)	(1)
		$\beta\text{-LUMO}$									
25911	0.4124	$\alpha\text{-HOMO}-$									
		$\alpha\text{-LUMO}$	27→30	27→30	4→16	8→1	11→4	1→6	11→4	8→1	1→7
		$\alpha\text{-HOMO-}$	(3)	(3)	(12)	(-7)	(-7)	(5)	(-7)	(-7)	(6)
		[$\alpha\text{-LUMO+2}$]									
31686	1.0785	[$\alpha\text{-HOMO-2}$] –									
		$\alpha\text{-LUMO}$									
		[$\alpha\text{-HOMO-1}$] –	44→44	44→44	1→1	1→1	4→2	0→1	4→2	1→1	1→6
		[$\alpha\text{-LUMO+1}$]	(0)	(0)	(0)	(0)	(-2)	(1)	(-2)	(0)	(5)
		[$\beta\text{-HOMO-1}$] –									
		[$\beta\text{-LUMO+1}$]									
[C]⁺											
10368	1.1694	HOMO – LUMO	47→14 (-33)	47→14 (-33)	2→0 (-2)	0→14 (14)	0→21 (21)	1→1 (0)	0→21 (21)	0→14 (14)	3→0 (-3)
13333	0.2112	[HOMO-1] –	43→14	43→14	1→1	1→14	5→21	0→1	5→21	1→14	0→0
		LUMO	(-29)	(-29)	(0)	(13)	(16)	(1)	(16)	(13)	(0)
29186	0.3221	[HOMO-1] –	43→16	43→16	1→14	1→1	5→5	0→11	5→5	1→1	1→31
		[LUMO+1]	(-27)	(-27)	(13)	(0)	(0)	(11)	(0)	(0)	(30)
29531	0.2022	[HOMO-13] –	30→16	30→16	12→1	5→13	1→20	7→1	1→20	5→13	10→1

		LUMO	(-14)	(-14)	(-11)	(8)	(19)	(-6)	(19)	(8)	(-9)
30346	0.3805	HOMO –	46→30	46→30	2→19	0→0	1→4	1→10	1→4	0→0	3→2
		[LUMO+2]	(-16)	(-16)	(17)	(0)	(3)	(9)	(3)	(0)	(-1)
[C]⁻											
16018	0.9501	HOMO – LUMO	12→46	12→46	1→1	11→0	26→0	1→0	26→0	11→0	0→6
			(34)	(34)	(0)	(-11)	(-26)	(-1)	(-26)	(-11)	(6)
19420	0.1739	HOMO –	12→48	12→48	1→1	11→2	26→1	1→0	26→1	11→2	0→-1
		[LUMO+1]	(36)	(36)	(0)	(-9)	(-25)	(-1)	(-25)	(-9)	(-1)
20725	0.1362	HOMO –	12→5	12→5	1→61	11→0	26→6	1→9	26→6	11→0	0→9
		[LUMO+2]	(-7)	(-7)	(60)	(-11)	(-20)	(8)	(-20)	(-11)	(9)
30534	1.5889	[HOMO-2] –	40→47	40→47	2→0	1→0	6→0	1→0	6→0	1→0	3→5
		LUMO	(7)	(7)	(-2)	(-1)	(-6)	(-1)	(-6)	(-1)	(2)

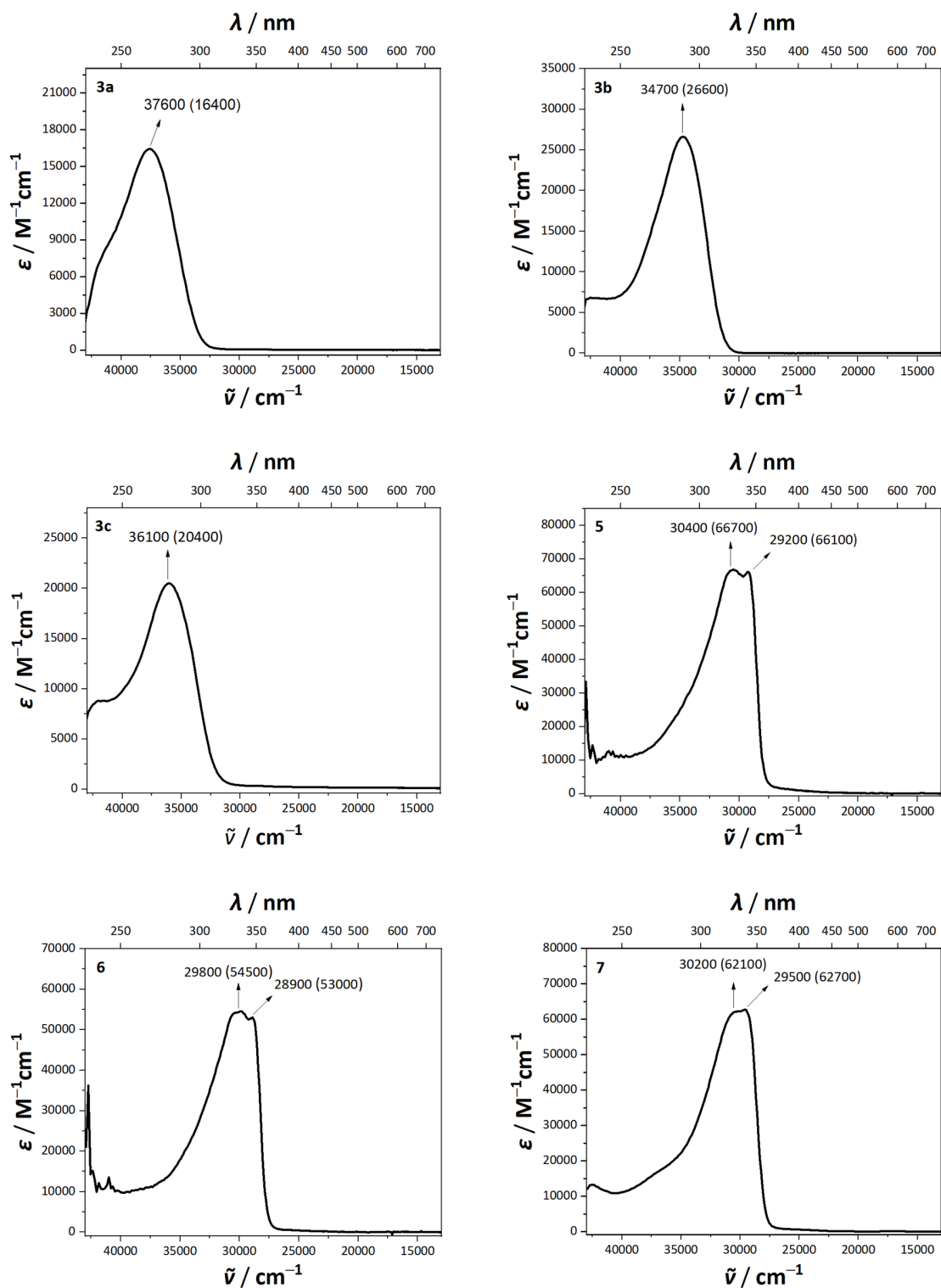


Figure S6. The UV-vis spectra ($\tilde{\nu}_{max} / \text{cm}^{-1}$ ($\epsilon / \text{M}^{-1}\text{cm}^{-1}$)) of tetrazines **3a – c, 5, 6** and **7**.

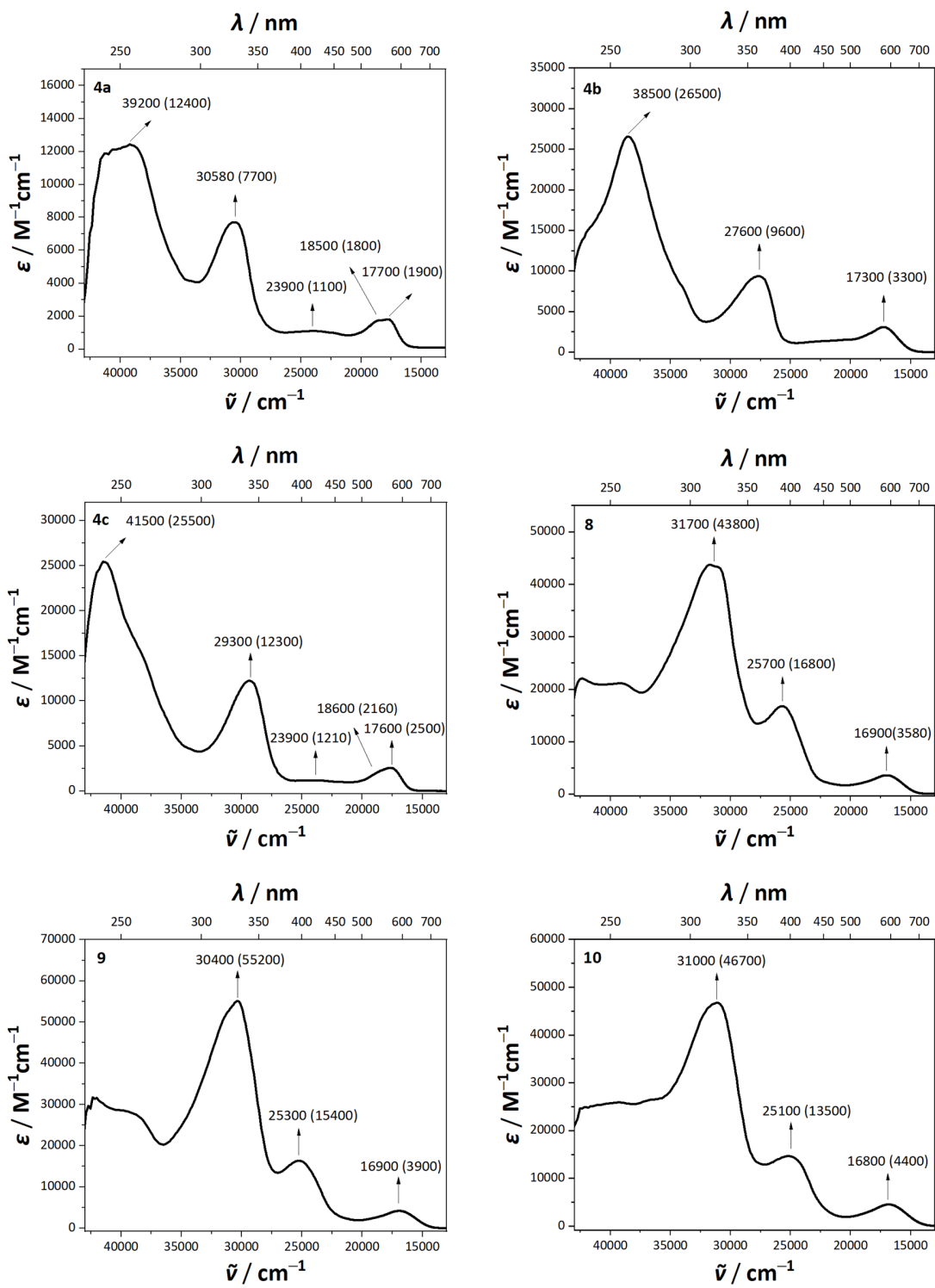


Figure S7. The UV-vis spectra ($\tilde{\nu}_{max} / \text{cm}^{-1}$ ($\epsilon / \text{M}^{-1}\text{cm}^{-1}$)) of verdazyls **4a – c**, **8**, **9** and **10**.

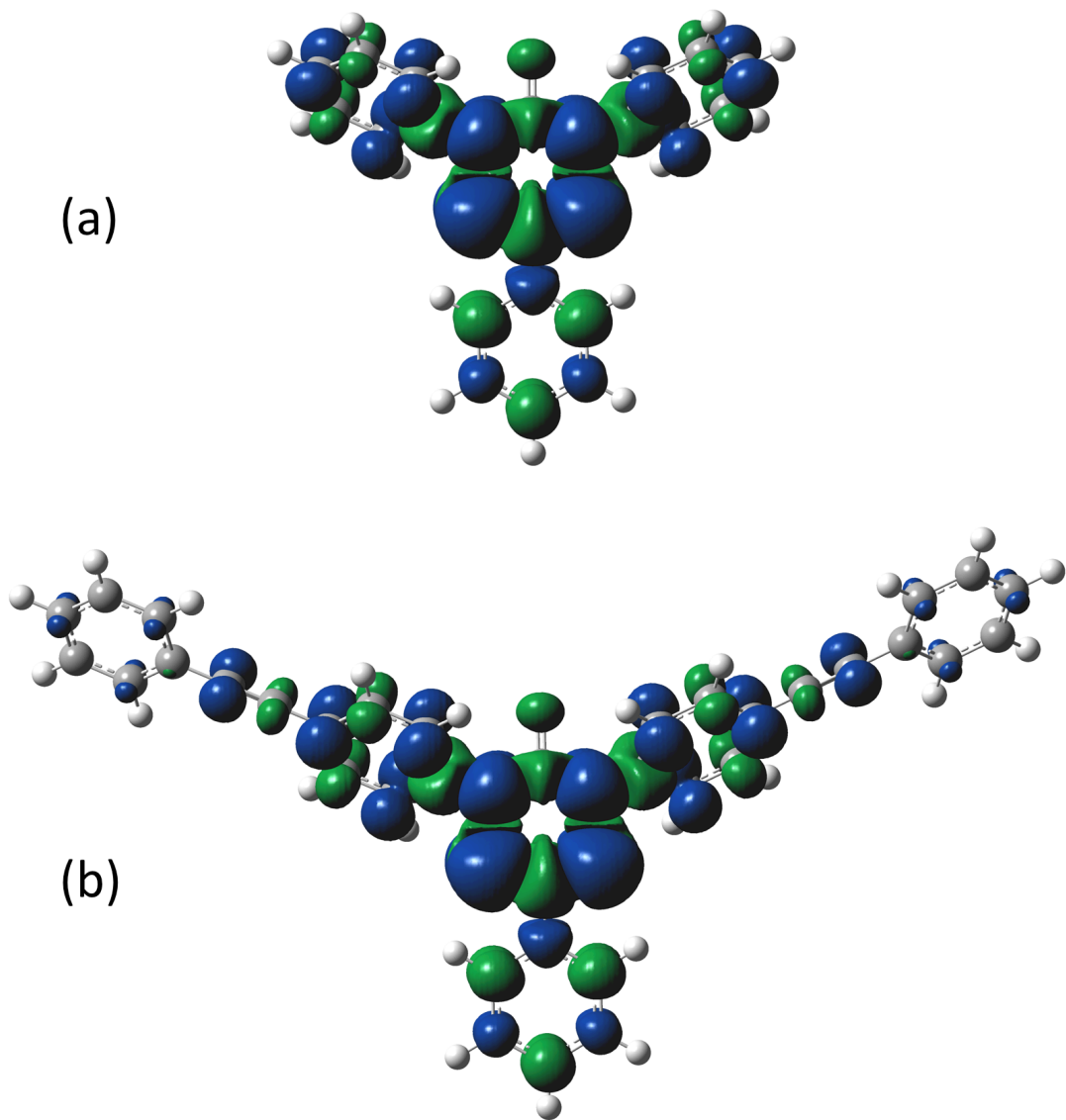


Figure S8. Plots of the spin density from the model verdazyl radical (a) [B] (b) [C]

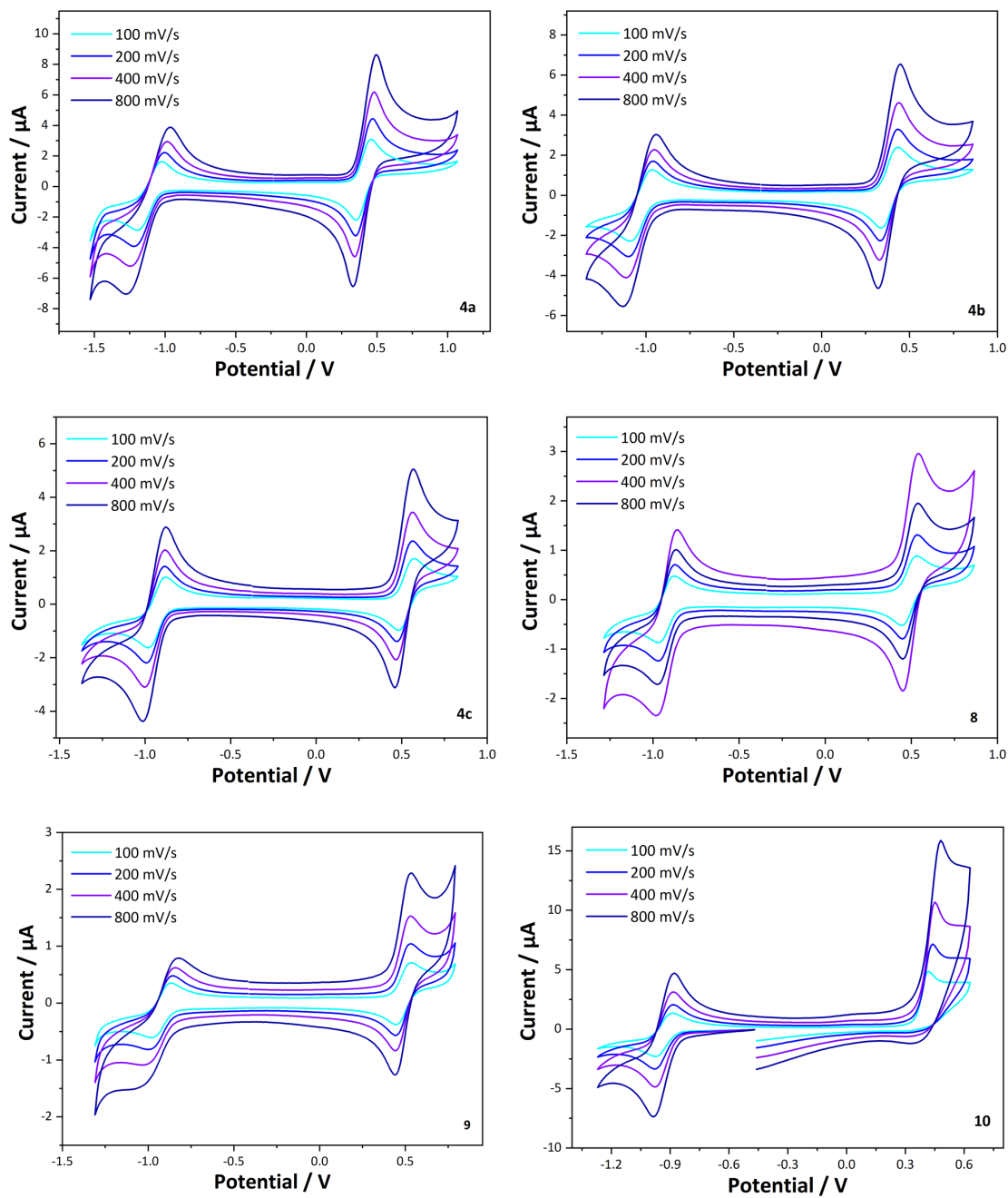


Figure S9. Cyclic Voltammograms of compounds **4a – c** and **8 – 10** in 0.1 M NBu₄PF₆ / CH₂Cl₂ solution. Voltammograms are plotted vs ferrocene/ferrocenium ($E_{1/2} = 0$ V) from data collected against an decamethylferrocene / decamethylferrocenium internal reference couple ($E_{1/2} = -0.55$ V).

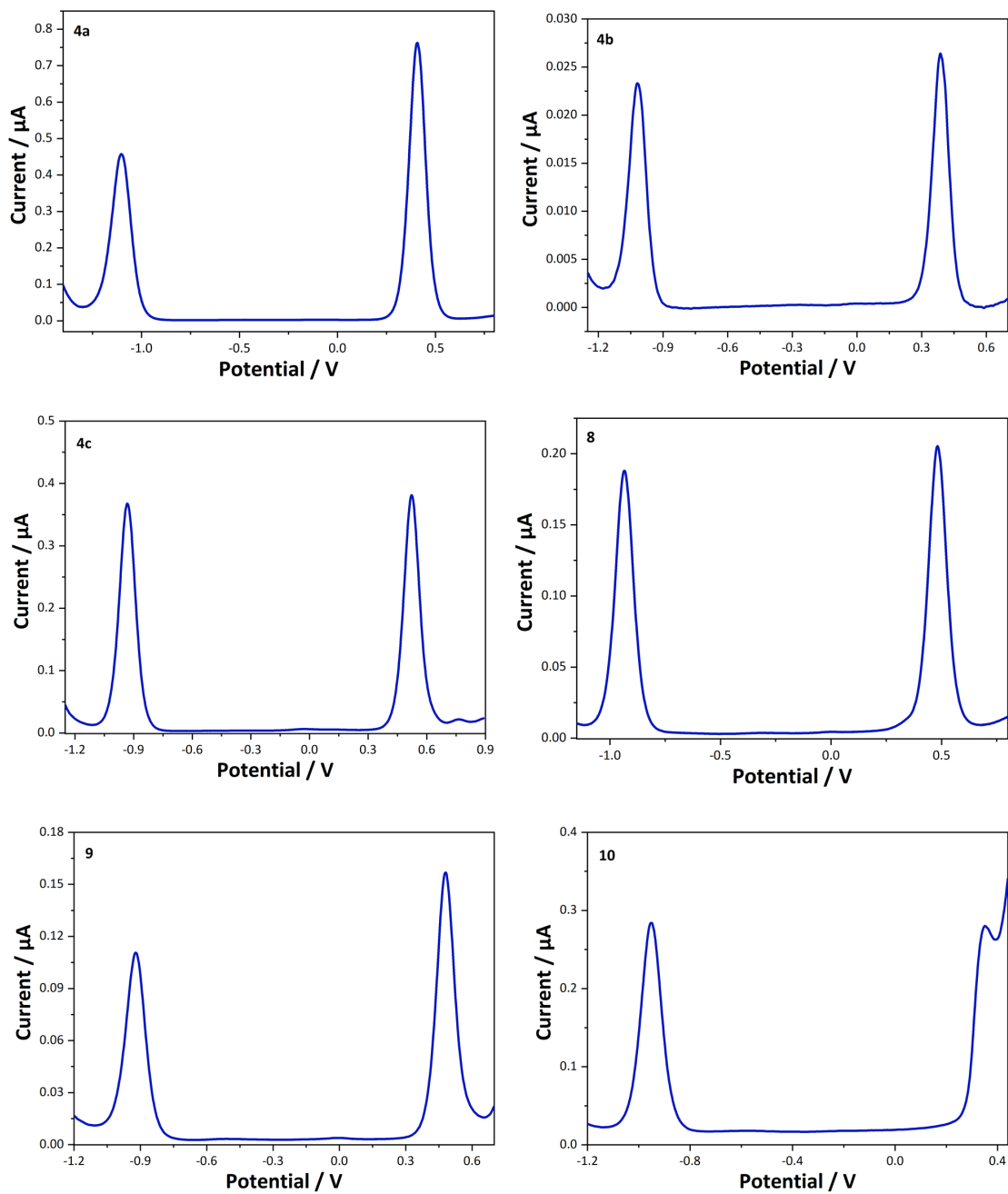


Figure S10. Square Wave Voltammograms of compounds **4a – c** and **8 – 10** in 0.1 M NBu₄PF₆ / CH₂Cl₂ solution. Voltammograms are plotted vs ferrocene/ferrocenium ($E_{1/2} = 0$ V) from data collected against a decamethylferrocene / decamethylferrocenium internal reference couple ($E_{1/2} = -0.55$ V).

Table S5. Summary of UV-vis-NIR spectroelectrochemical data for compounds **4a-c**, **9** and **10**.

Compound	Experimental ν /cm ⁻¹ (ϵ / dm ³ mol ⁻¹ cm ⁻¹)		
	[x] ⁺	[x]	[x] ⁻
4a	21460 (5200), 15800 (10300)	39200 (14000), 30580 (7700), 18500 (1800), 17700 (1900)	38400 (17500), 26900 (4800)
4b	36900 (23900), 15400 (8400), 11860 (16800)	38500 (26500), 27600 (9600), 17300 (3300)	36900 (22500), 25000 (6600)
4c	40500 (20400), 18900 (7080), 15360 (13020)	41500 (25500), 29300 (12300), 18600 (2160), 17600 (2500)	25300 (10300)
9	30300 (44900), 11600 (9400)	30400 (55200), 25300 (15400) 16900 (3900)	30300 (75300)
10	—	31000 (46700), 25100 (13500), 16800 (4400)	30800(53400)

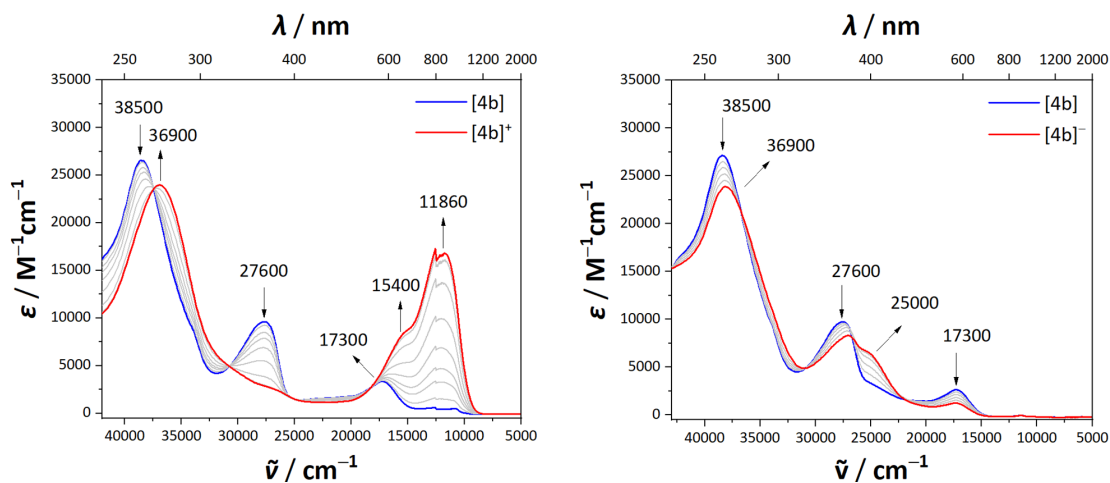


Figure S11. Plots of spectroelectrochemical data of **4b** in the UV-vis-NIR region.

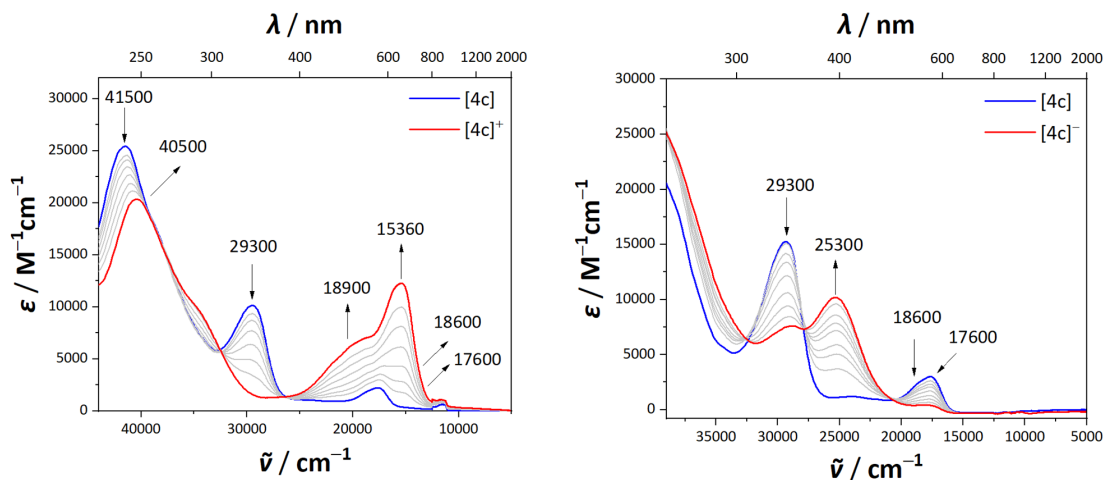


Figure S12. Plots of spectroelectrochemical data of **4c** in the UV-vis-NIR region.

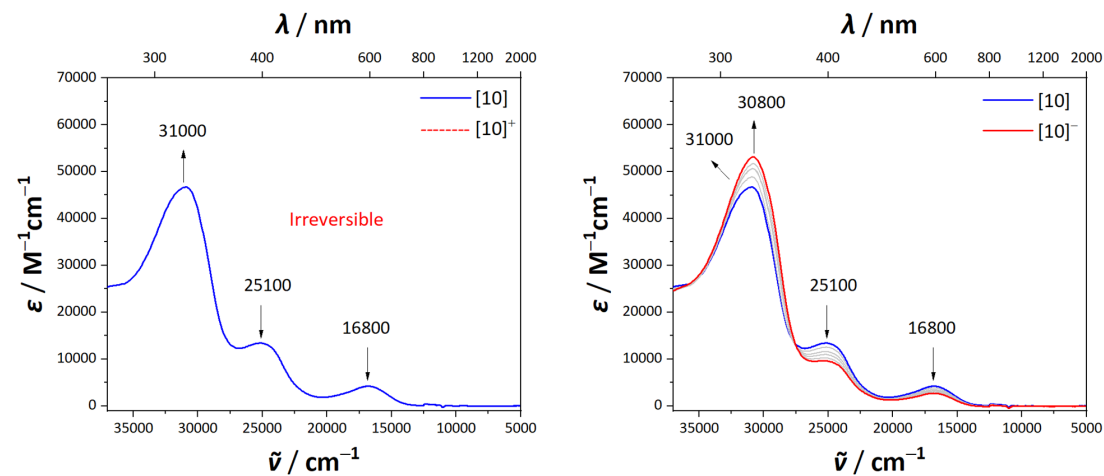


Figure S13. The spectroelectrochemically generated spectra of **[10]⁻**.

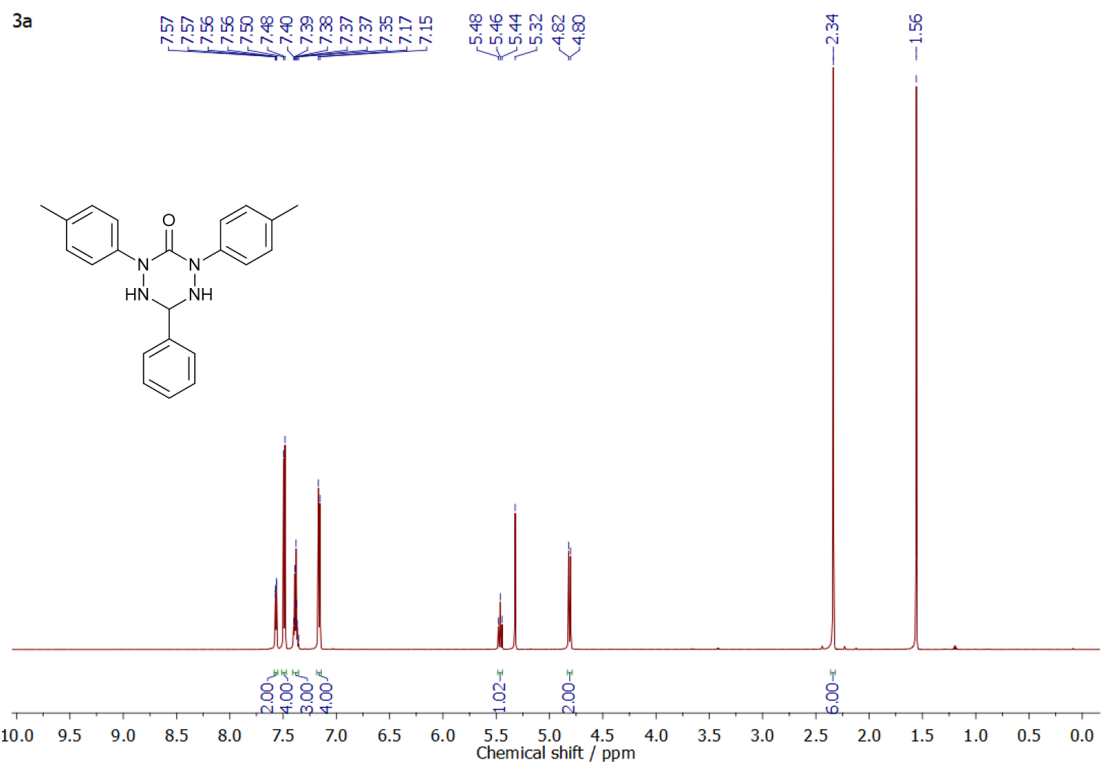


Figure S14. The ^1H NMR spectrum of 3a.

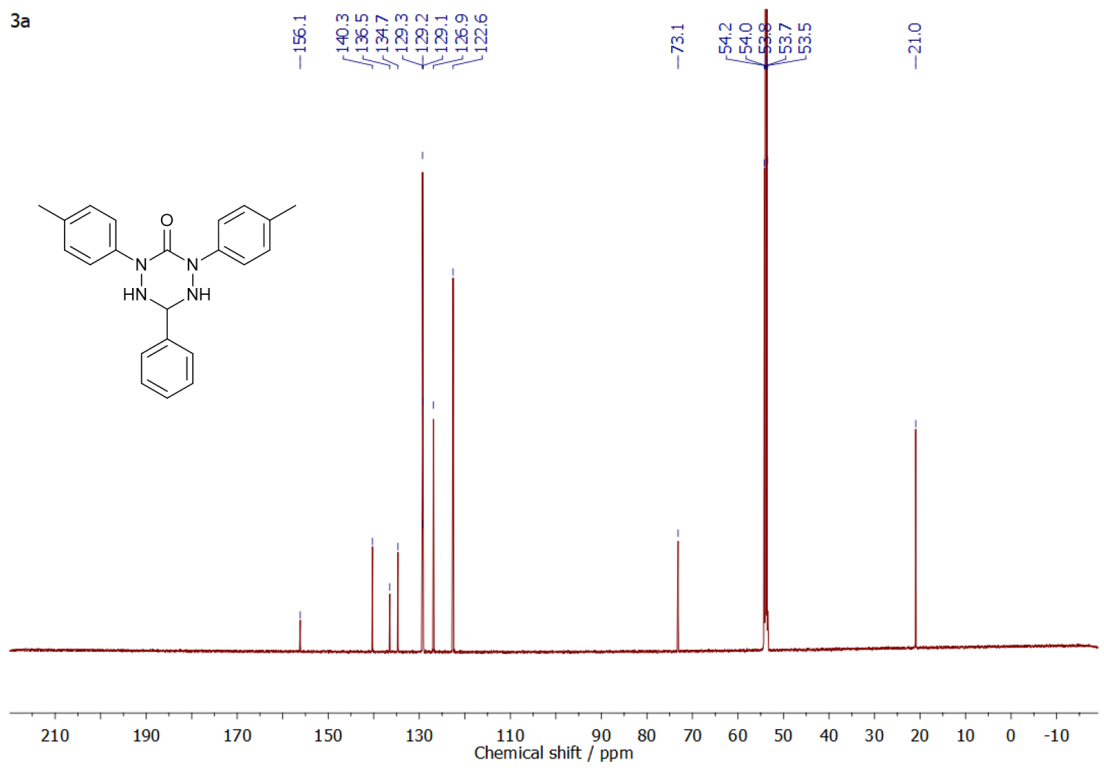


Figure S15. The $^{13}\text{C}\{^1\text{H}\}$ NMR spectrum of **3a**.

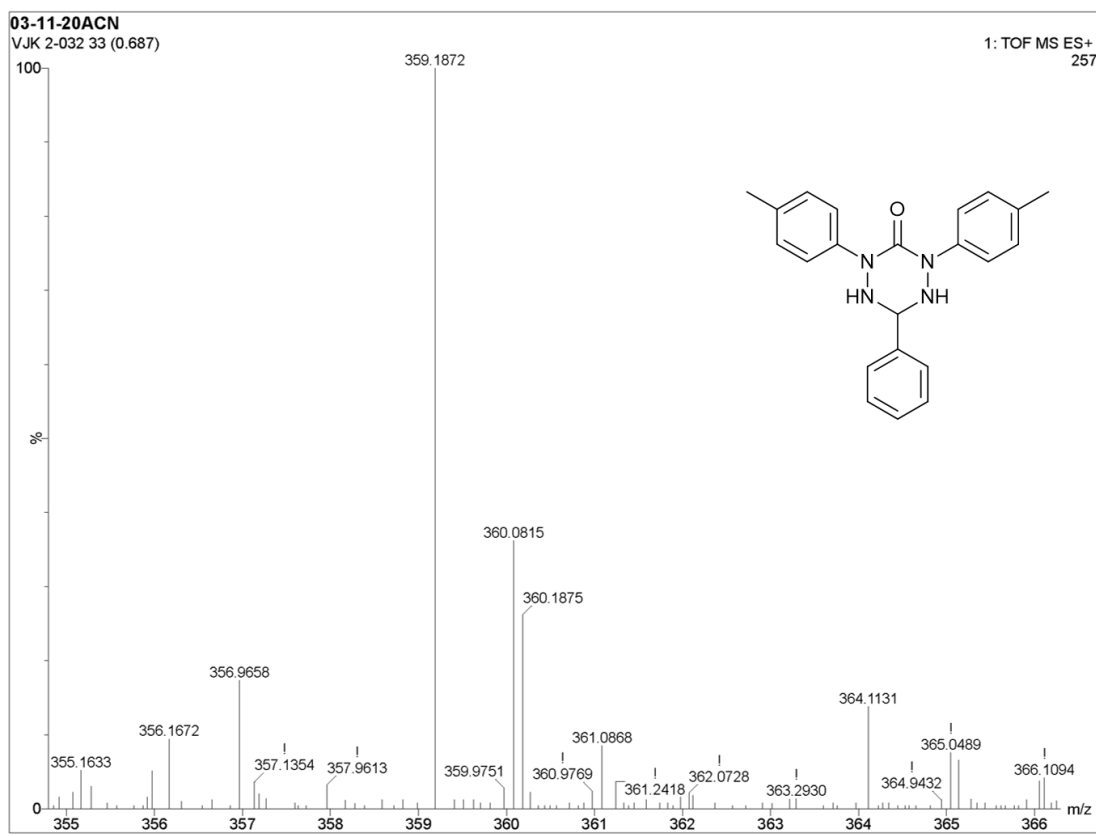


Figure S16. The mass spectrum of **3a**.

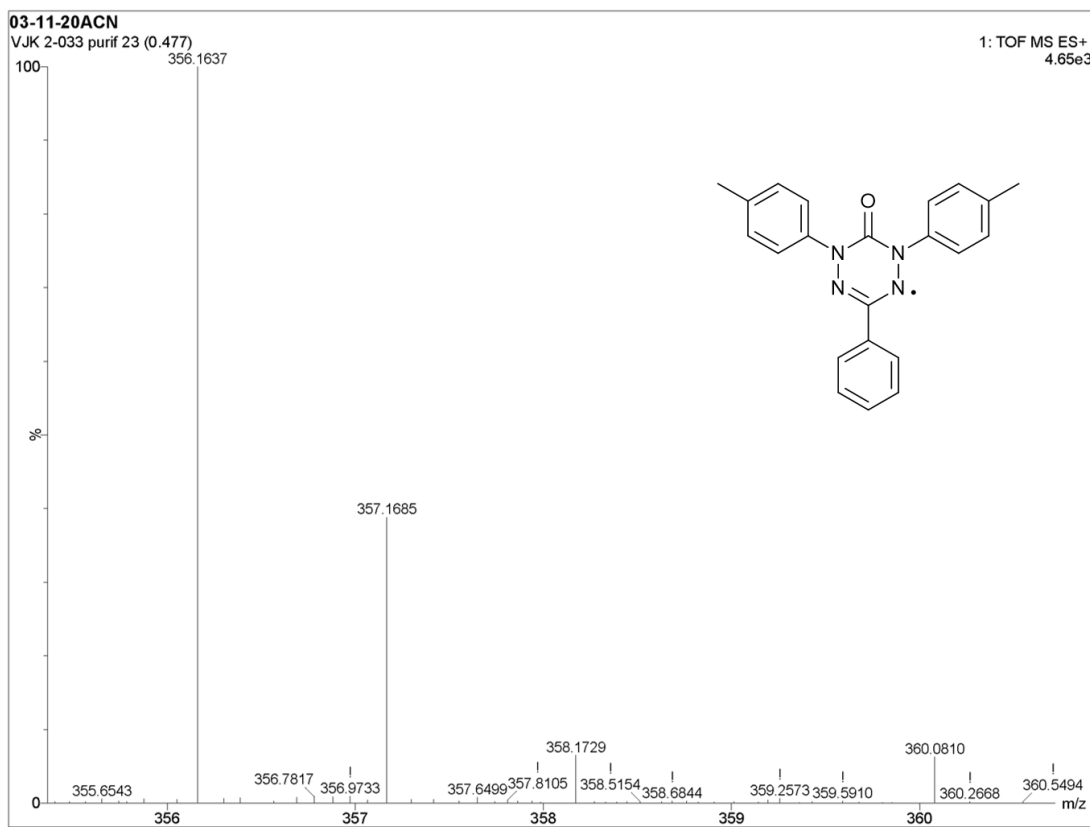


Figure S17. The mass spectrum of **4a**.

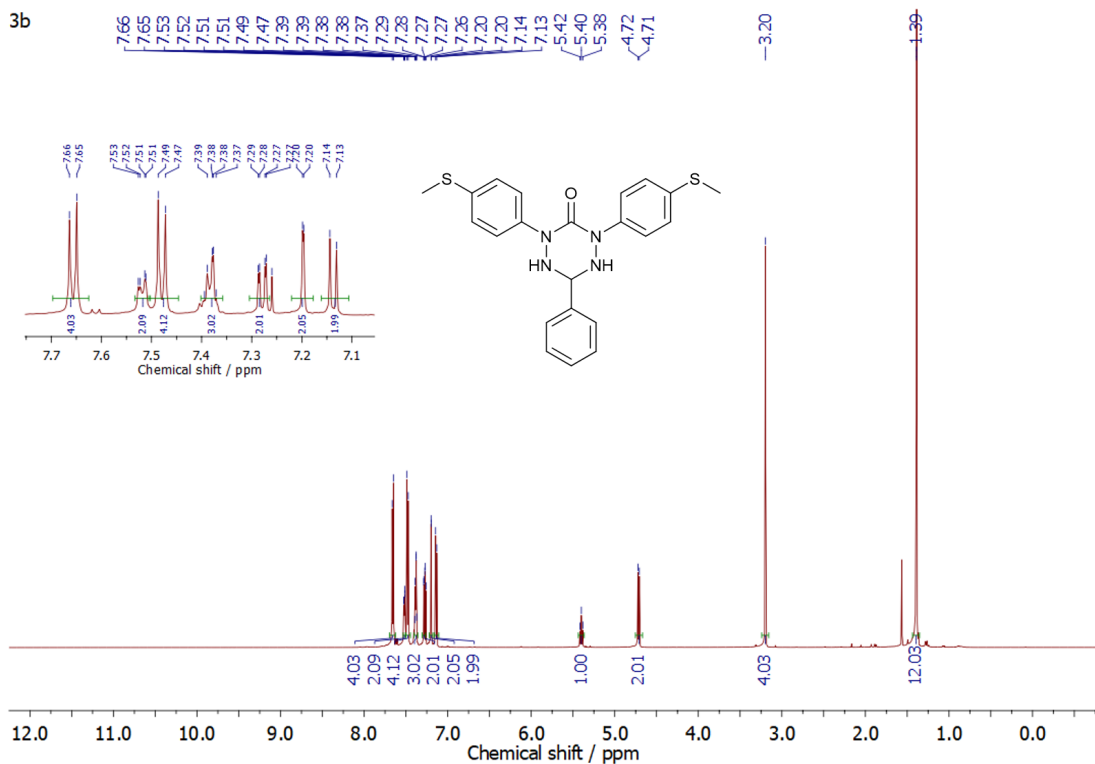


Figure S18. The ¹H NMR spectrum of **3b**. The inset shows an expansion of the aromatic region for clarity.

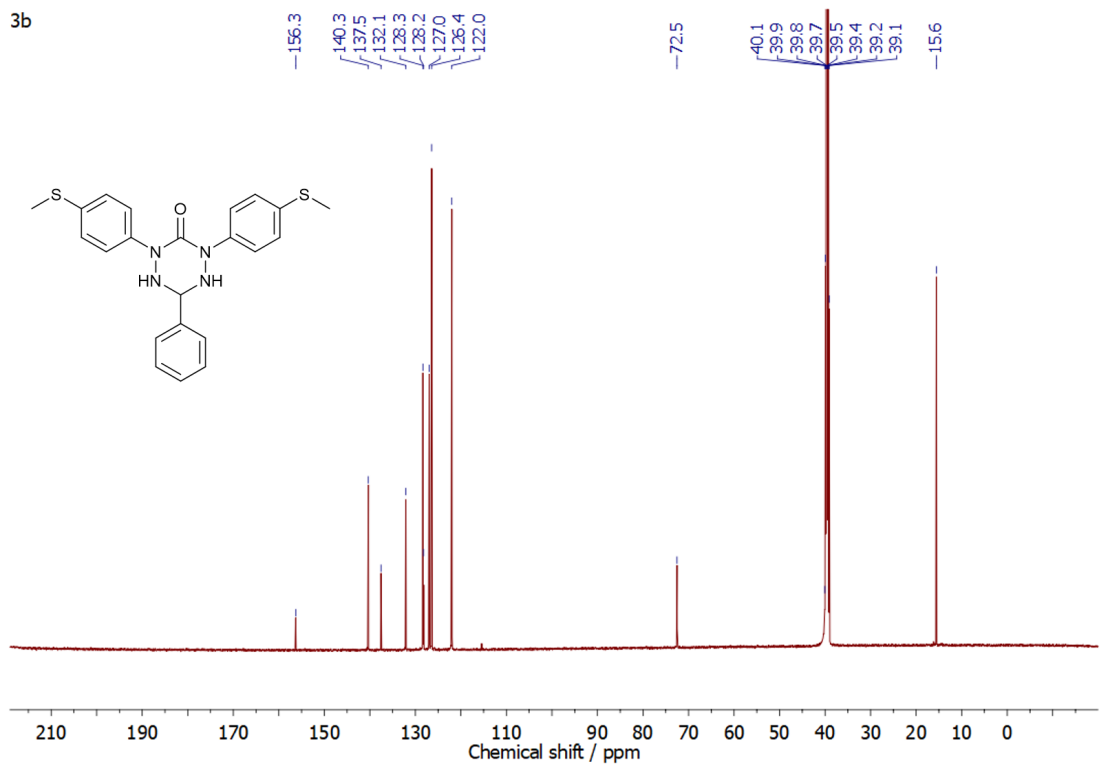


Figure S19. The $^{13}\text{C}\{^1\text{H}\}$ NMR spectrum of **3b**.

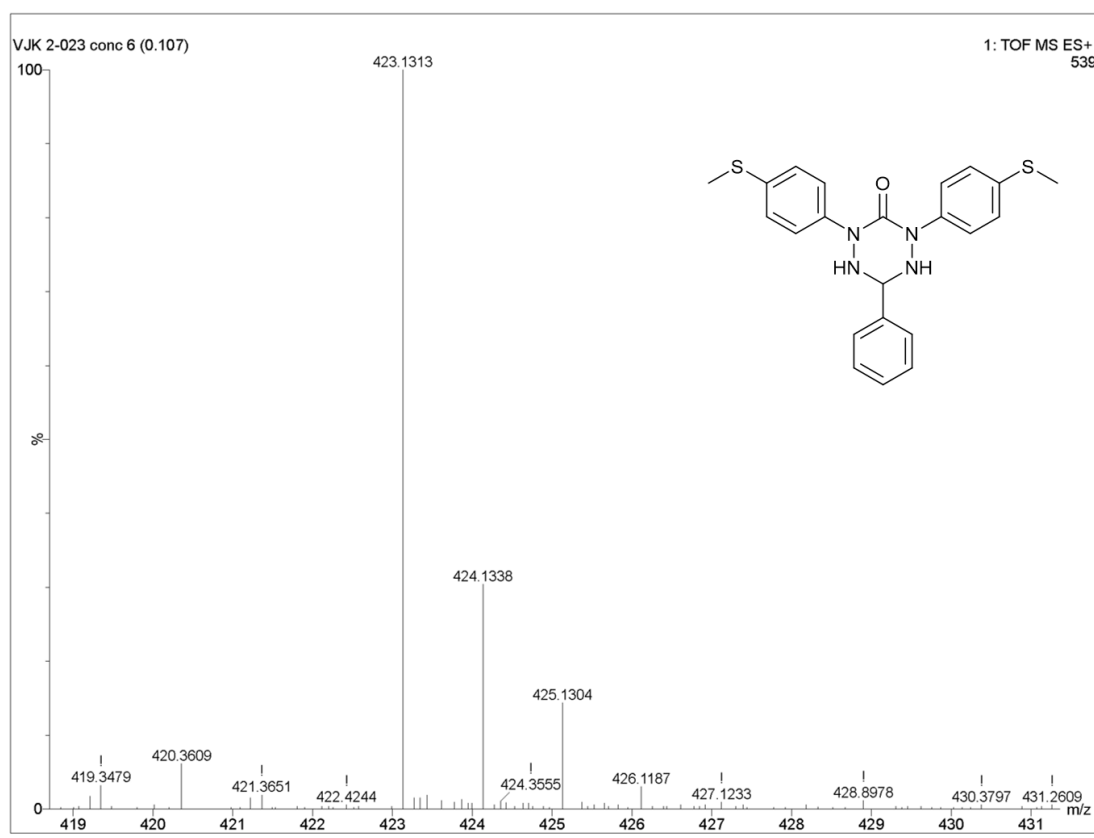


Figure S20. The mass spectrum of **3b**.

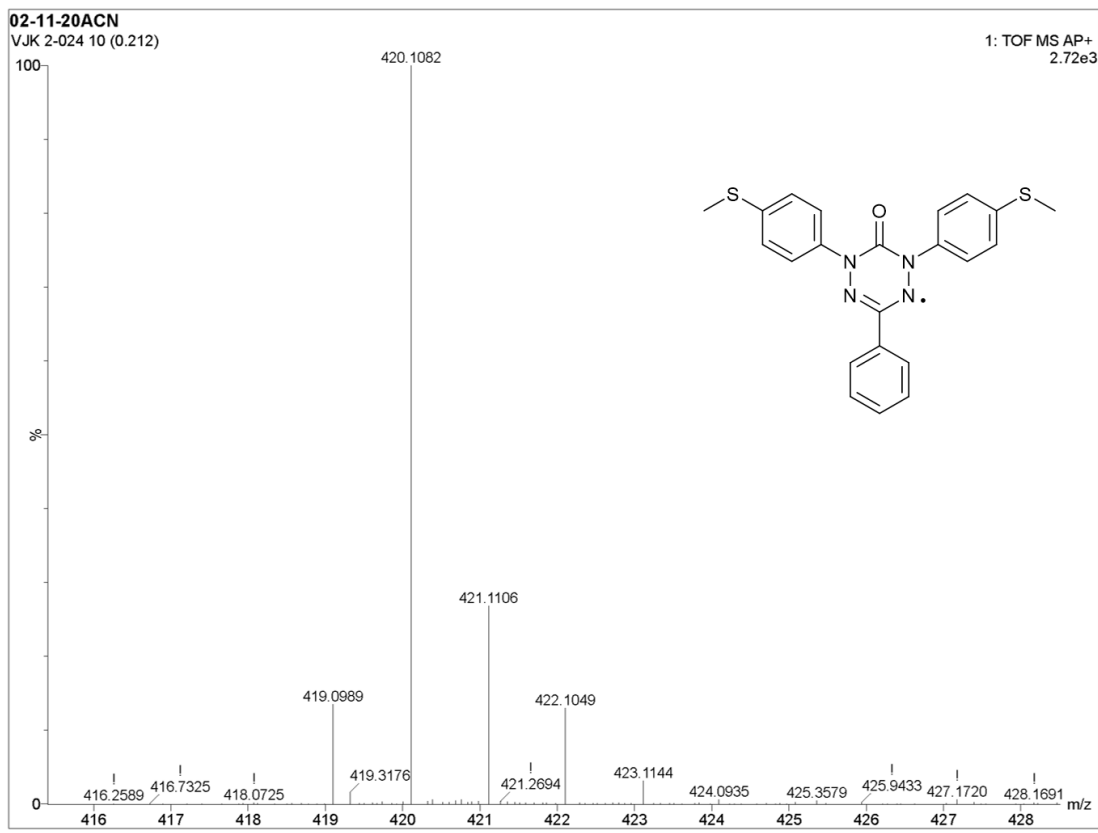


Figure S21. The mass spectrum of **4b**.

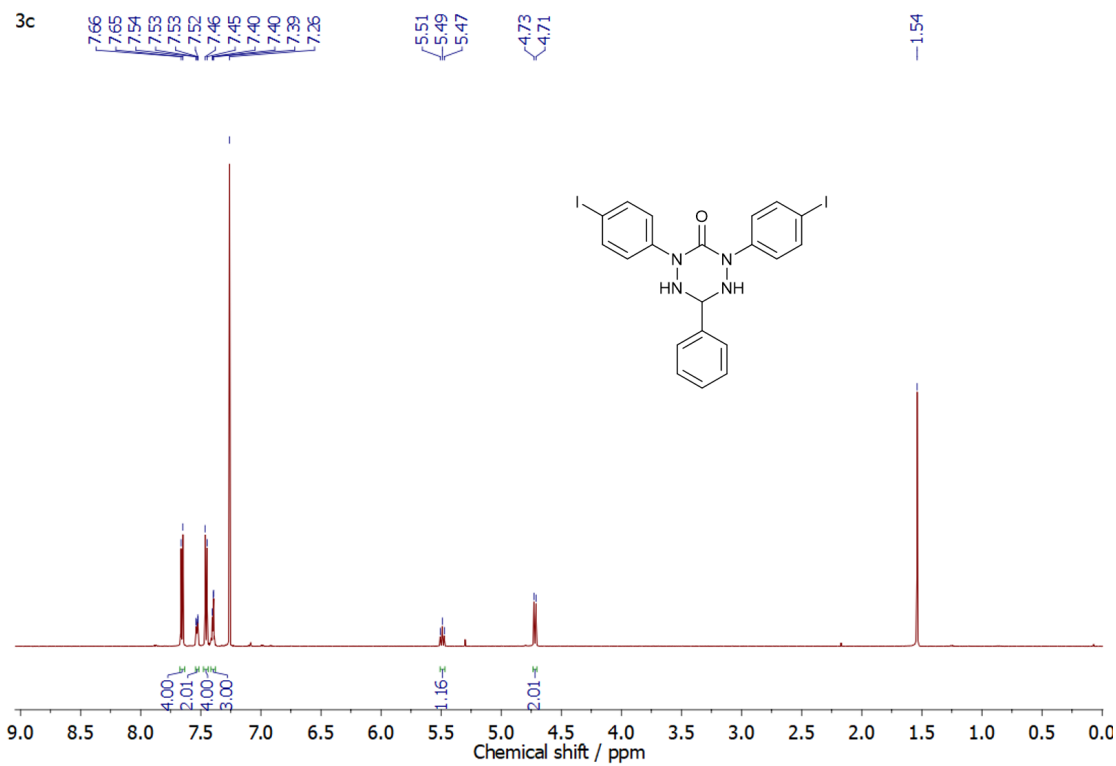


Figure S22. The ^1H NMR spectrum of **3c**. The inset shows an expansion of the aromatic region for clarity.

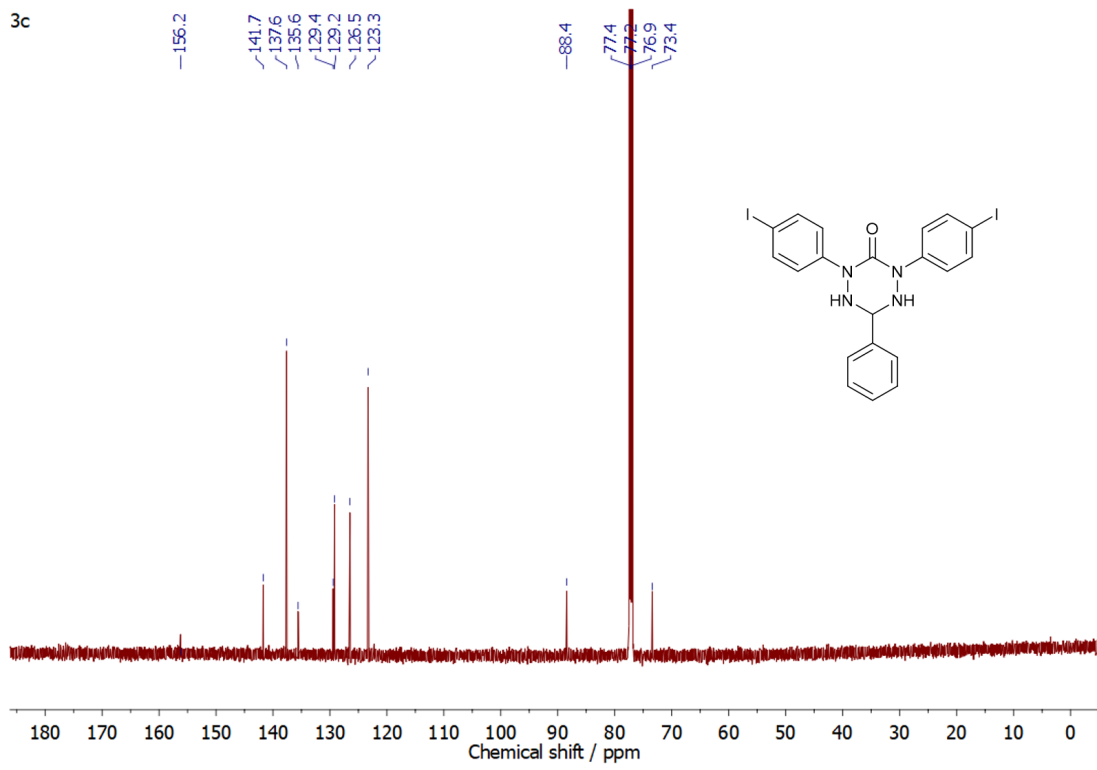


Figure S23. The $^{13}\text{C}\{^1\text{H}\}$ NMR spectrum of **3c**.

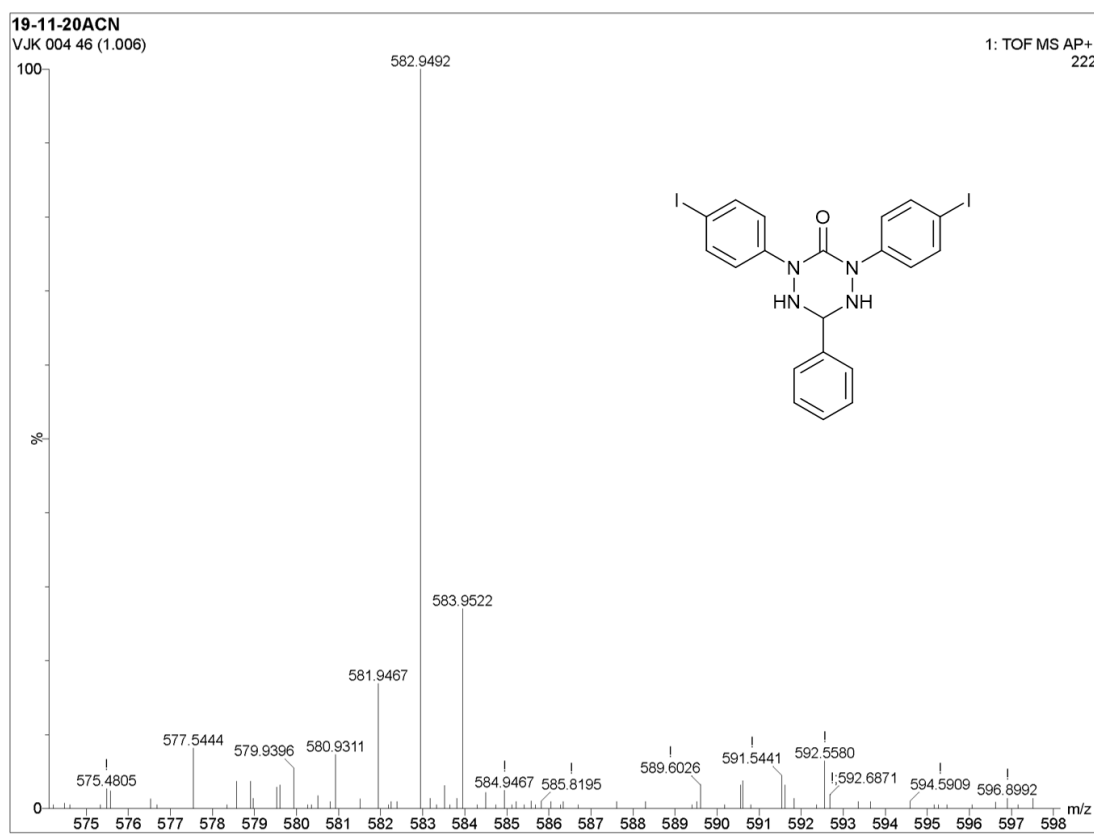


Figure S24. The mass spectrum of **3c**.

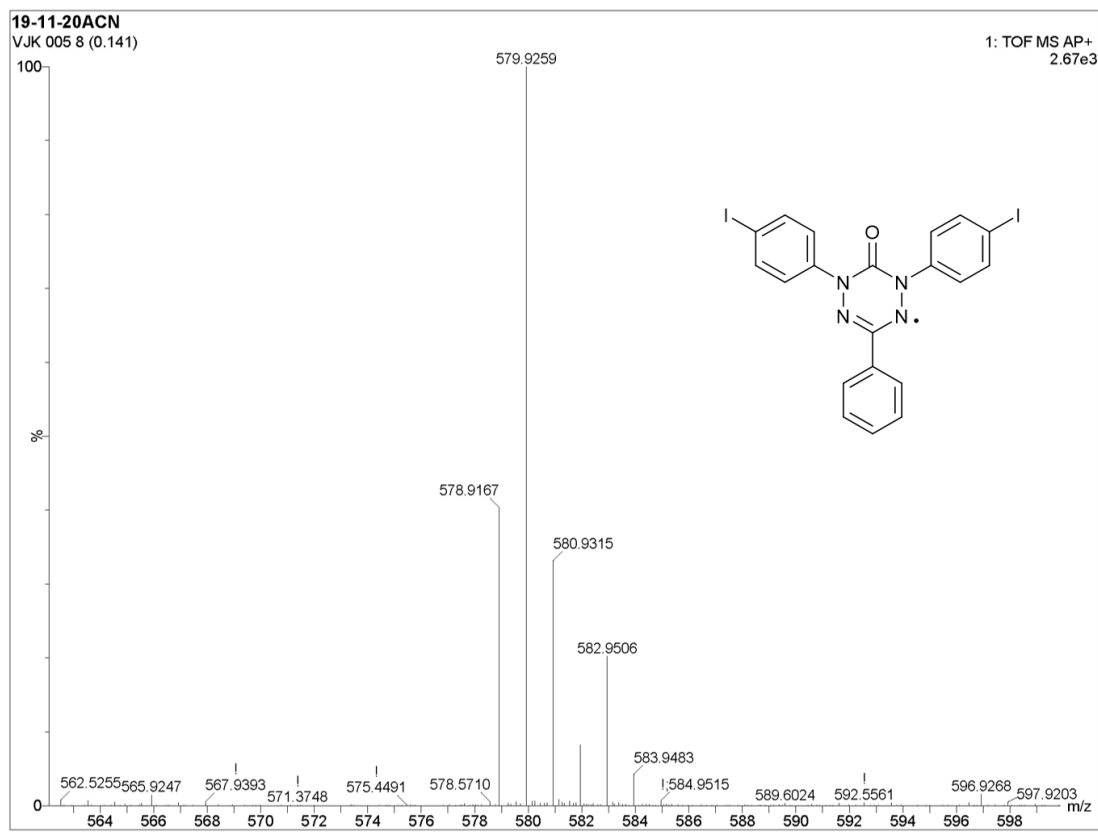


Figure S25. The mass spectrum of **4c**.

5

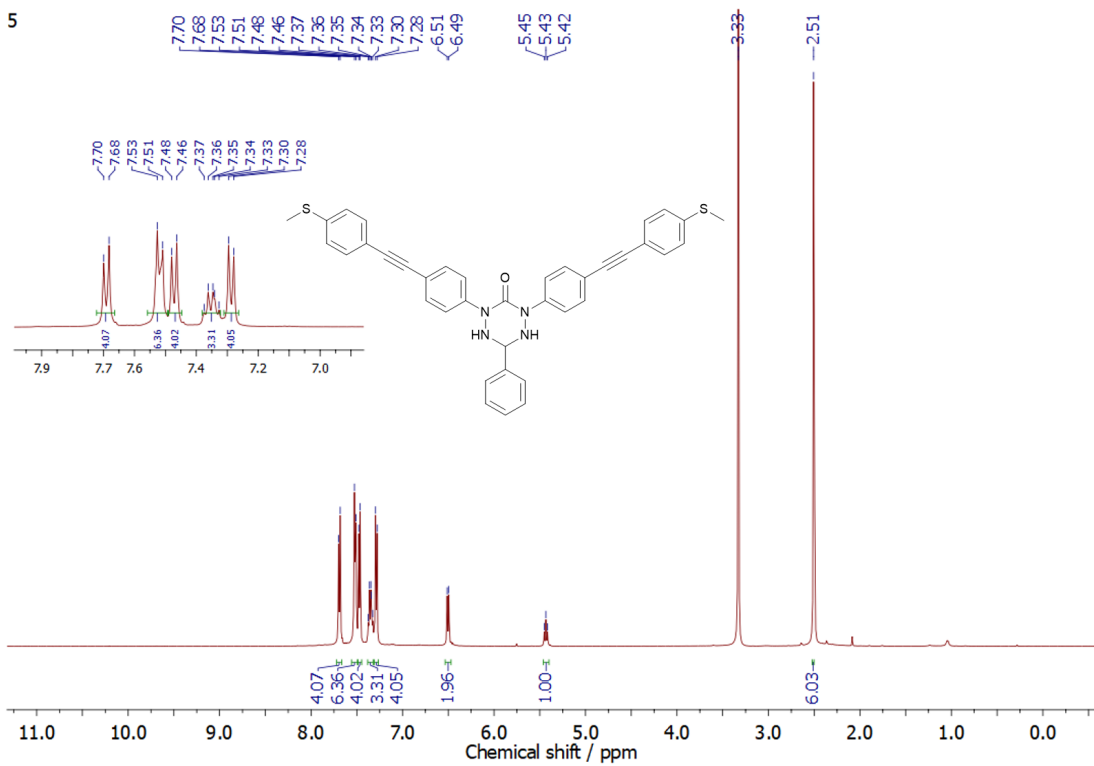


Figure S26. The ¹H NMR spectrum of **5**. The inset shows an expansion of the aromatic region for clarity.

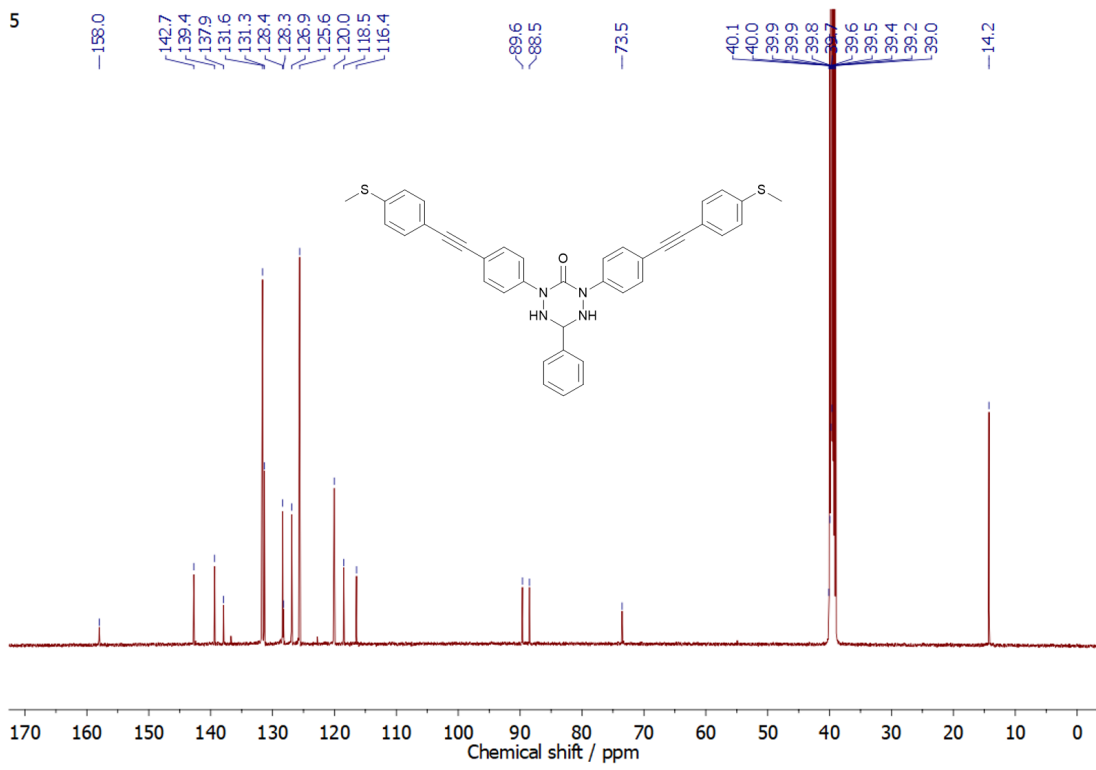


Figure S27. The $^{13}\text{C}\{^1\text{H}\}$ NMR spectrum of **5**.

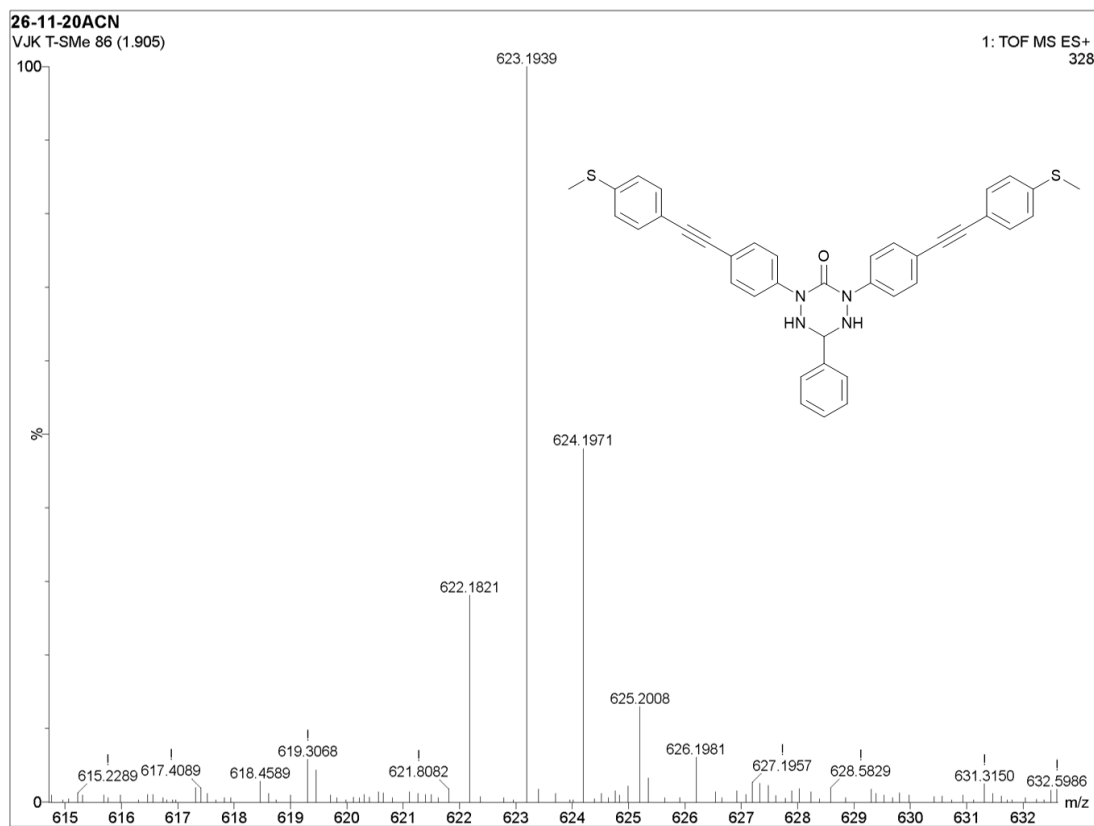


Figure S28. The mass spectrum of **5**.

6

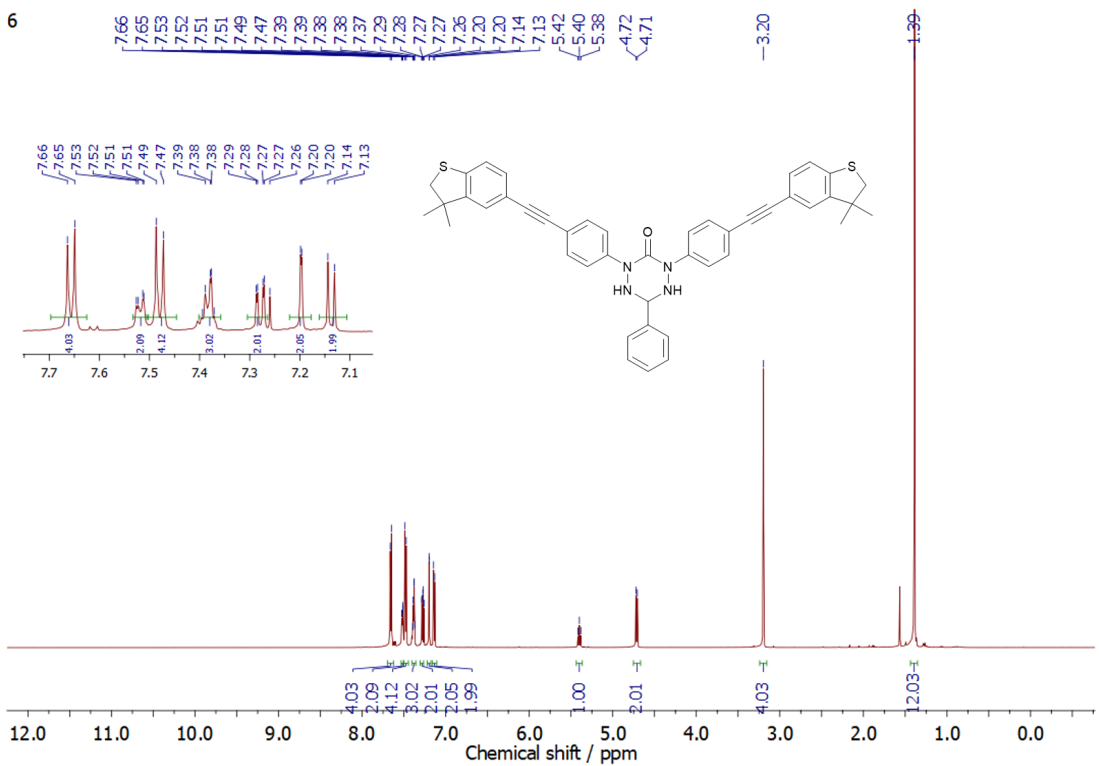


Figure S29. The ^1H NMR spectrum of **6**. The inset shows an expansion of the aromatic region for clarity.

6

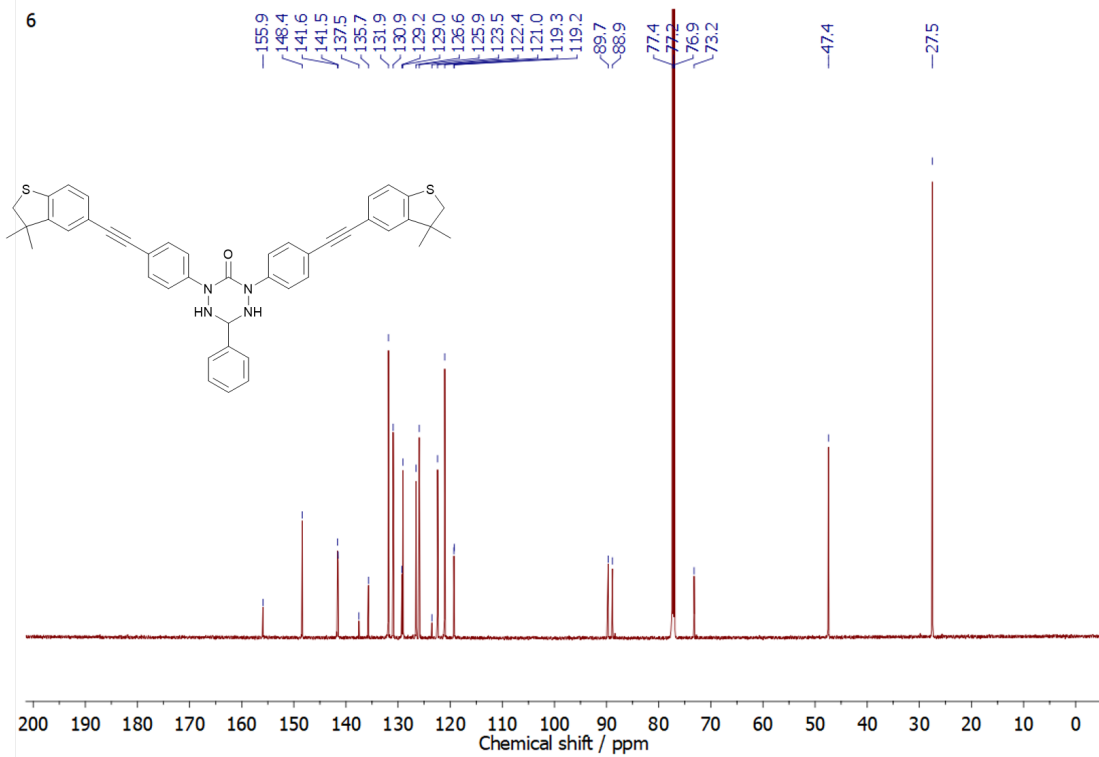


Figure S30. The $^{13}\text{C}\{^1\text{H}\}$ NMR spectrum of **6**.

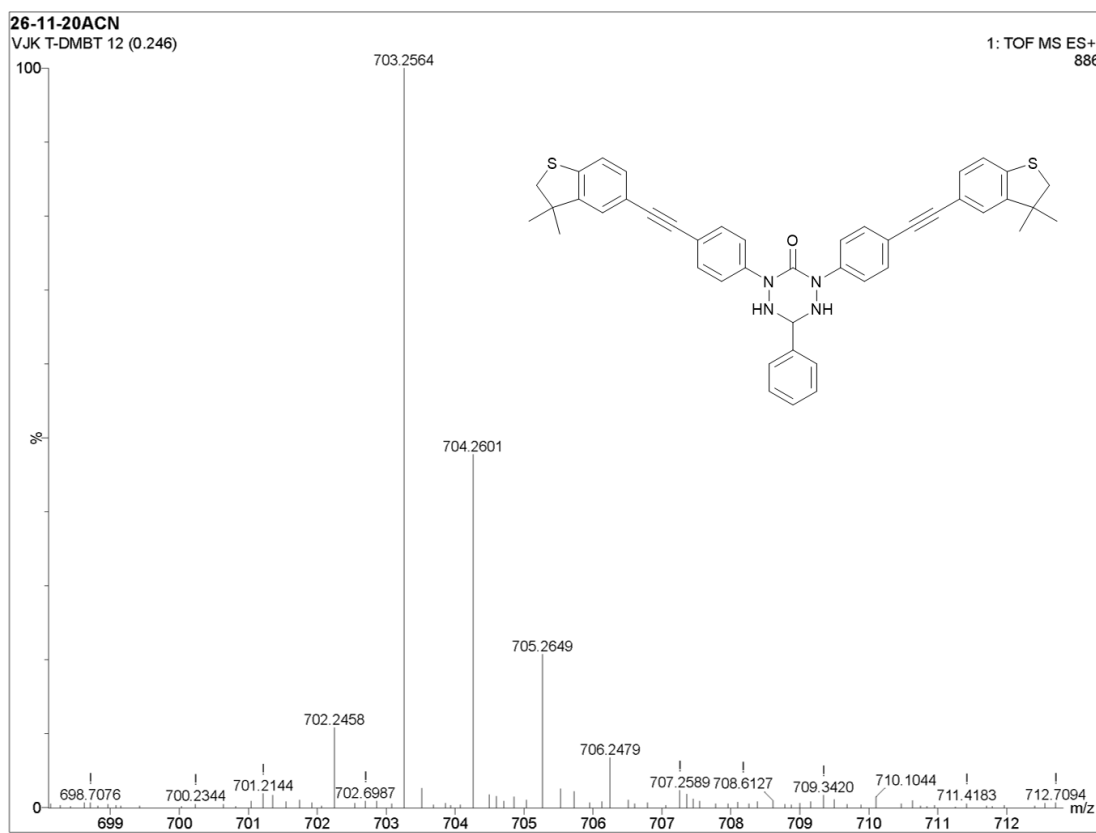


Figure S31. The mass spectrum of 6.

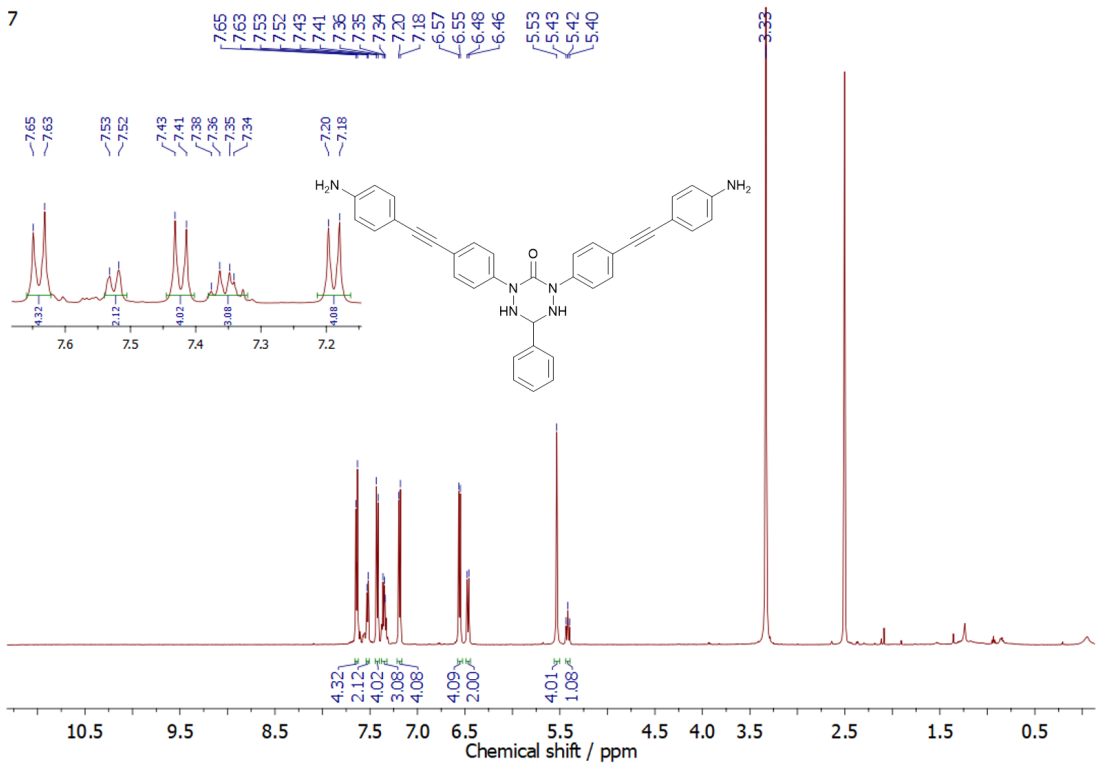


Figure S32. The ¹H NMR spectrum of 7. The inset shows an expansion of the aromatic region for clarity.

7

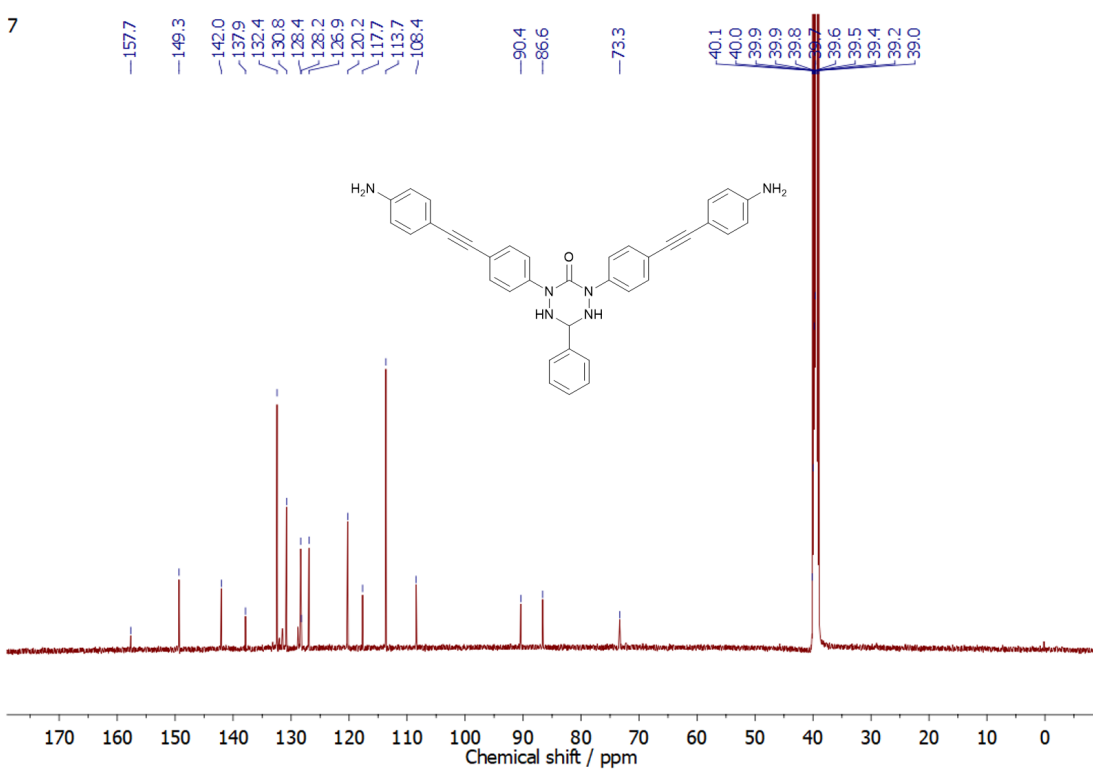


Figure S33. The $^{13}\text{C}\{^1\text{H}\}$ NMR spectrum of 7.

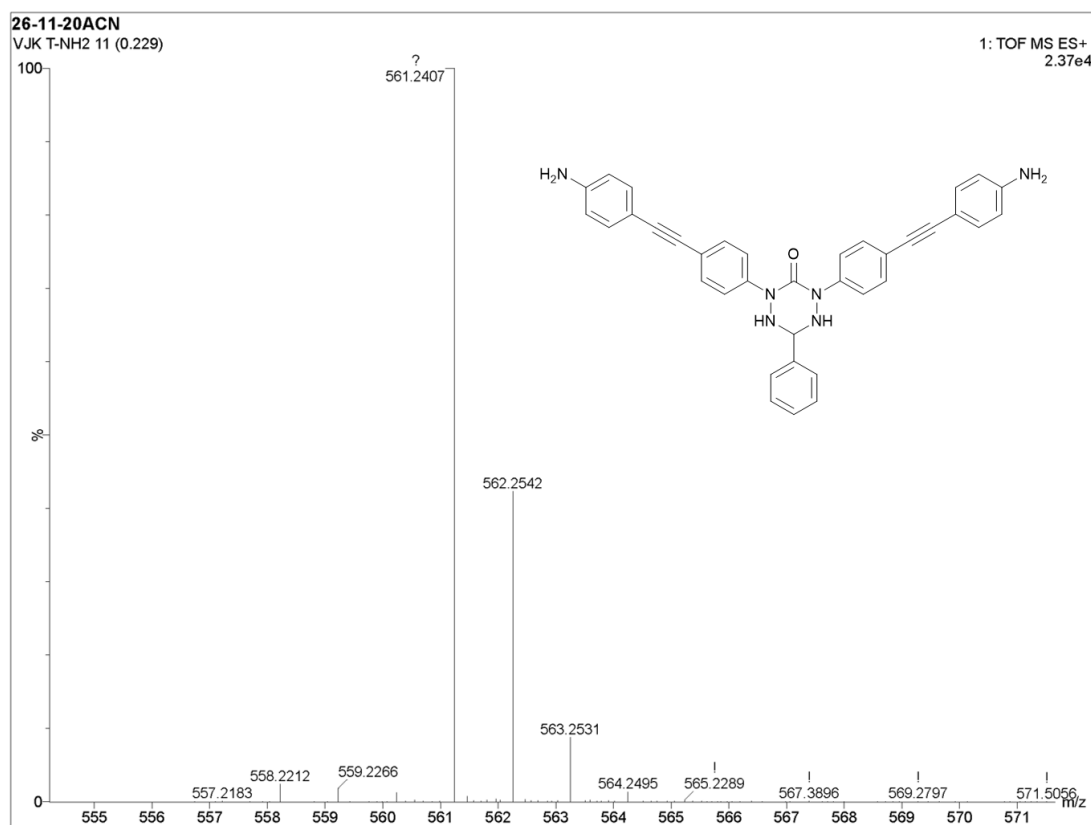


Figure S34. The mass spectrum of 7.

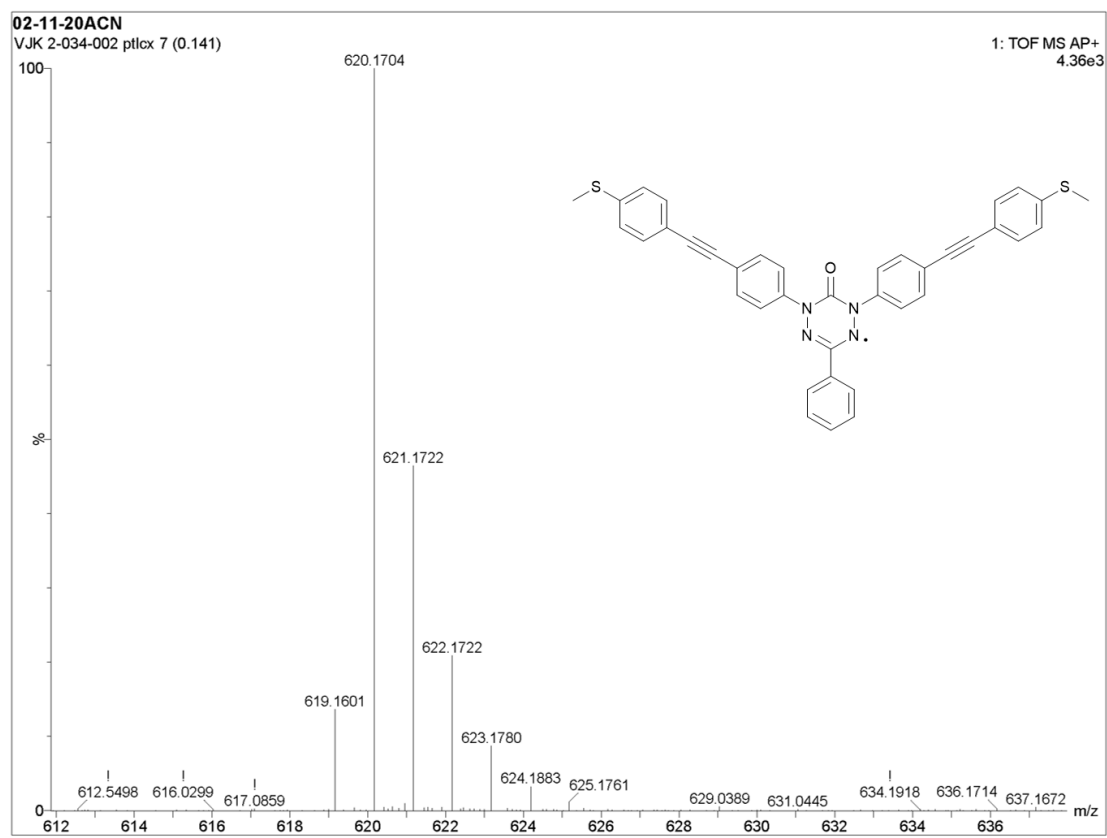


Figure S35. The mass spectrum of **8**.

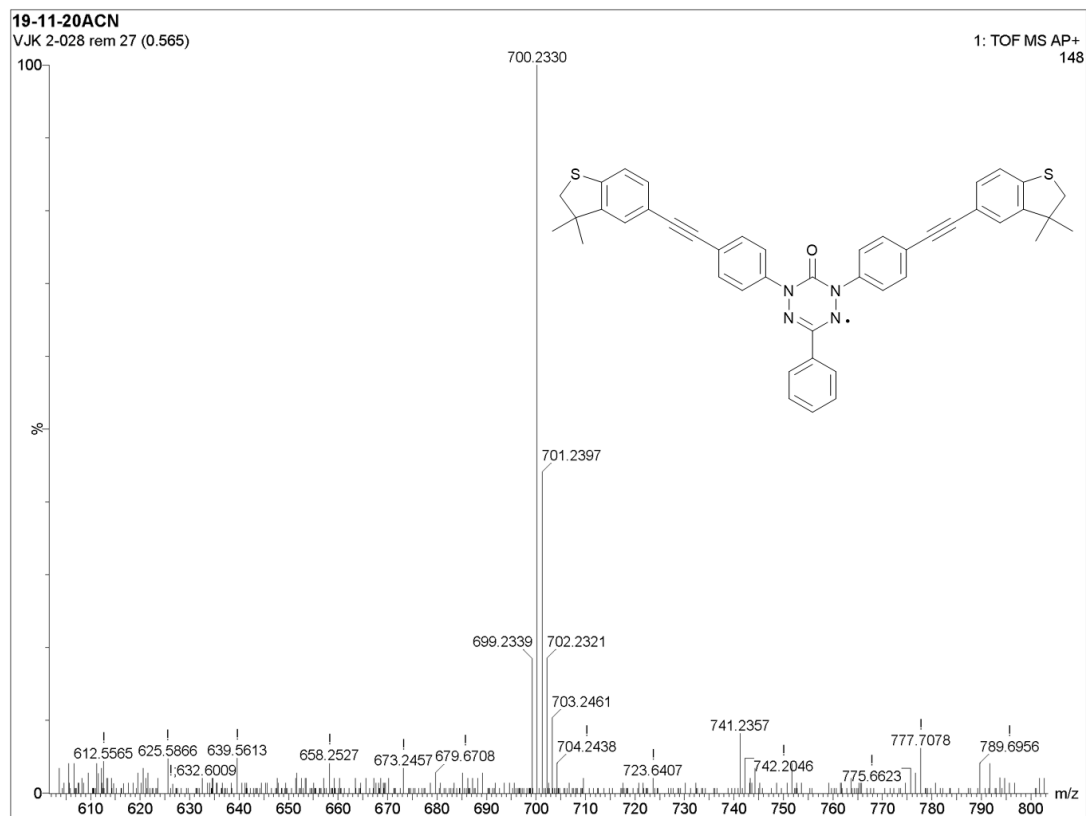


Figure S36. The mass spectrum of **9**.

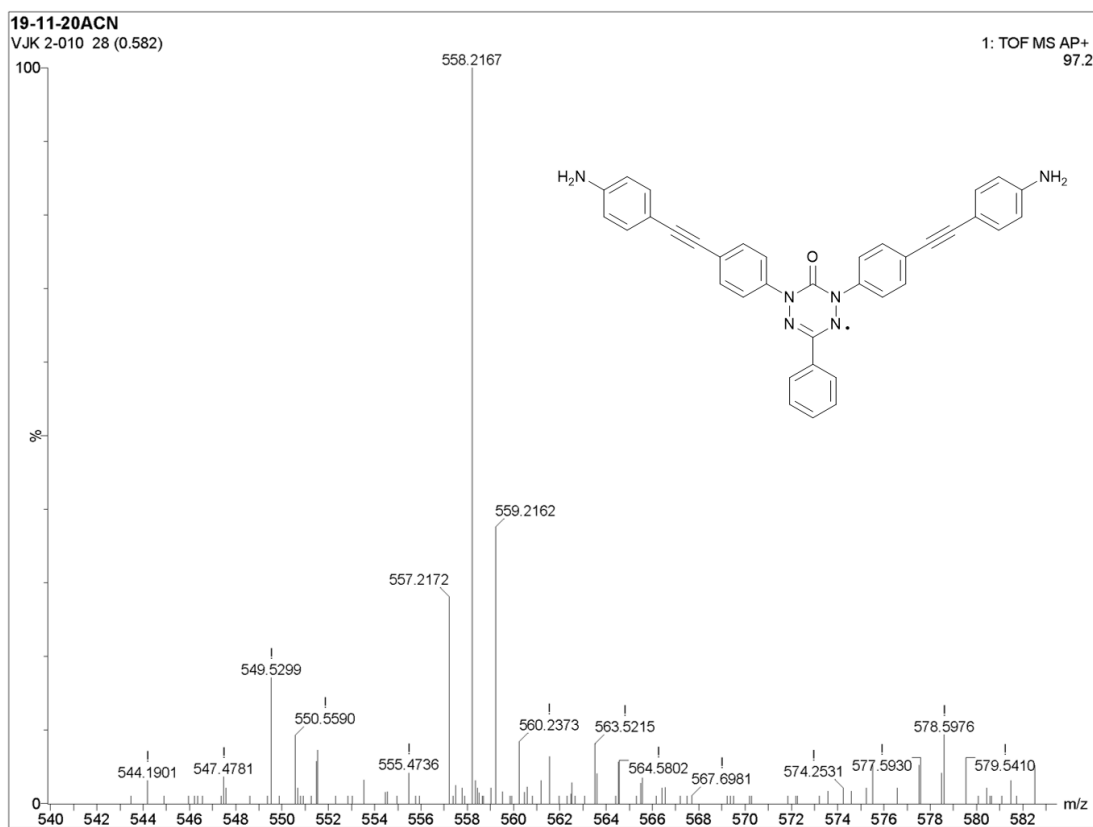


Figure S37. The mass spectrum of **10**.

Additional EPR materials and Methods

A basis set that describes the radical spin manifold can be built from the product of the eigenstates of the interacting electron ($S = 1/2$) and nuclear (^{14}N , $I = 1$) spins:

$$|S \quad M\rangle \otimes |I_1 \quad m_1\rangle \otimes |I_2 \quad m_2\rangle \otimes |I_3 \quad m_3\rangle \otimes |I_4 \quad m_4\rangle \quad \text{Eq. 1}$$

Here, S refers to the electronic spin state, M refers to the electronic magnetic sublevel, I_i refers to the nuclear spin state of ^{14}N , and m_i refers to the nuclear magnetic sublevels of each ^{14}N . S take the value of $\frac{1}{2}$ and M the values $\pm 1/2$. I_i the value of 1 and m_i the values -1, 0 and +1. The spin Hamiltonian that describes the spin manifold is:

$$\hat{H} = g\beta_e \vec{B}_0 \cdot \vec{S} + \sum_{i=1}^4 (-g_n \beta_n \vec{B}_0 \cdot \vec{I}_i + a_i \vec{S} \cdot \vec{I}_i) \quad \text{Eq. 2}$$

It contains (i) an electronic Zeeman term describing the unpaired electron's interaction with the applied magnetic field (g), (ii) a nuclear Zeeman term for each ^{14}N nucleus and the applied magnetic field, and (iii) an electron-nuclear hyperfine term (a_i) for each ^{14}N nucleus describing the magnetic interaction between the unpaired electron and each nucleus. Note that the nuclear quadrupole term does not need to be considered when simulation the EPR spectrum.

Owing to the symmetry of the oxoverdazyl framework, the four ^{14}N hyperfine couplings represent two equivalent sets: two larger couplings a_1 and a_2 ; and two smaller couplings a_3 and a_4 . In the text, Figure 9 and Table 2, a_1 and a_2 are described by the label $a(\text{N}_{2,3})$ and a_3 and a_4 are described by the label $a(\text{N}_{1,4})$ which makes use of the crystallographic labelling of the four nitrogen sites (Scheme 3).